https://doi.org/10.5194/egusphere-2026-1263
Preprint. Discussion started: 7 April 2026

A Physics-based Framework to Infer Firn Properties on Antarctic Ice Shelves from ASCAT Observations

Shashwat Shukla[1], Bert Wouters[1], Sanne Veldhuijsen[2], Sophie de Roda Husman[1], Weiran Li[1], and Stef Lhermitte[1,3]

[1]Department of Geoscience and Remote Sensing, Delft University of Technology, 2628 CD Delft, The Netherlands
[2]Institute for Marine and Atmospheric Research Utrecht, Utrecht University, 3584CS Utrecht, The Netherlands
[3]Department of Earth and Environmental Sciences, KU Leuven, 3000 Leuven, Belgium

Correspondence: Shashwat Shukla (s.shukla@tudelft.nl)

Abstract. The stability of Antarctic ice shelves is closely linked to the properties of the firn layer, which regulates meltwater retention and influences ice shelf vulnerability to hydrofracturing. Firn Densification Models (FDMs) provide valuable insights into the firn structure, but key properties such as grain size are often parameterized using simple approximations, leading to significant uncertainties, especially in regions lacking in-situ validation. Here, we leverage 15 years (2007–2021) of active microwave observations from the C-band Advanced Scatterometer (ASCAT) to infer an effective firn grain-size parameter across Antarctic ice shelves. Within this framework, we use the Institute for Marine and Atmospheric Research Utrecht Firn Densification Model (IMAU-FDM) to prescribe the state of the firn layer (layer thickness, density, temperature, and liquid water content) and couple it with the Snow Microwave Radiative Transfer (SMRT) model to simulate radar backscatter. Grain size is treated as an unknown microstructural parameter and is optimized by minimizing the misfit between FDM–SMRT simulations and ASCAT observations. The framework is further used to examine how the sensitivity of ASCAT backscatter varies across firn regimes, and how this influences the interpretation of backscatter in terms of FAC. Our results show broad consistency between optimized effective grain size and IMAU-FDM estimates in high-Firn Air Content (FAC) regions, where ASCAT backscatter is most sensitive to interannual variability in grain size. In contrast, larger discrepancies emerge in intermediate- to low-FAC regions, particularly on the Amery Ice Shelf, where ice saturation in the firn (pore-space depletion) influences grain growth. The sensitivity experiments indicate that inversion constraints are regime-dependent, with the strongest sensitivity to grain size in intermediate firn regimes and weaker constraints in strongly depleted firn. Furthermore, by statistically reducing grain-size-driven scatter after inversion, we present a proof of concept for a more interpretable backscatter–FAC relationship. These findings provide a basis for improving firn model parameterization and advancing large-scale monitoring of firn evolution across Antarctic ice shelves in a warming climate.

1 Introduction

Assessing firn properties is crucial for understanding the stability of Antarctic ice shelves, as firn regulates meltwater retention and influences their susceptibility to hydrofracturing (Kuipers Munneke et al., 2014). With climate warming intensifying surface melting, tracking firn evolution is essential for predicting the long-term stability of Antarctic ice shelves (Veldhuijsen

https://doi.org/10.5194/egusphere-2026-1263
Preprint. Discussion started: 7 April 2026

et al., 2024). Key firn properties, such as grain size and Firn Air Content (FAC; the vertically integrated pore-air content of the firn column), provide critical insights into firn microstructure and permeability, influencing its ability to store and refreeze meltwater (Kuipers Munneke et al., 2014; Picard et al., 2022b; Amory et al., 2024). In high-FAC firn, fresh snowfall maintains permeability, allowing meltwater to percolate and either refreeze within the firn or be stored internally (Kuipers Munneke et al., 2014). However, sustained melt and densification can deplete pore space, leading to ice-saturated firn conditions in which infiltration is strongly limited, promoting the formation of surface melt ponds that increase the risk of hydrofracturing and ice-shelf destabilization (Scambos et al., 2000).

Spatio-temporal variations in firn properties, specifically grain size and FAC, can be assessed using Firn Densification Models (FDMs) (Veldhuijsen et al., 2024; Medley et al., 2022), field-based methods (Clerx et al., 2022; Xu et al., 2023), and, to some extent, satellite observations (Alley et al., 2018; Scambos et al., 2003). FDMs provide a powerful means to simulate firn structure at high vertical and temporal resolution (Veldhuijsen et al., 2024), enabling reconstructions of FAC evolution over the contemporary Antarctic climate (Veldhuijsen et al., 2024; Medley et al., 2022). However, a critical limitation of FDMs is their simplistic treatment of grain size evolution, which is often parameterized with minimal observational constraints (Veldhuijsen et al., 2024). Although FDMs incorporate firn densification physics, they rely on assumed relationships between grain size and environmental conditions, which are poorly validated in regions with substantial melt-refreezing processes. This gap in model representation limits our ability to assess firn permeability, meltwater retention, and ice shelf vulnerability.

Satellite remote sensing provides a valuable opportunity to assess firn properties at large spatial scales, particularly using microwave observations that penetrate the snowpack and respond to variations in microstructure and therefore also grain size and FAC (Alley et al., 2018; Picard et al., 2022b). Active microwave backscatter from the C-band Advanced Scatterometer (ASCAT) is especially sensitive to firn microstructure and can be leveraged to improve grain size parameterization in FDMs. Previous studies (Alley et al., 2018) have explored ASCAT backscatter as a proxy for hydrofracture potential by examining the relationship between scattering properties and surface mass balance (SMB) components, such as melt season duration and accumulation, to assess firn saturation. Alternatively, Dattler et al. (2024) demonstrated an end-to-end, physics-based workflow from passive microwave observations, snow microwave radiative transfer model (SMRT), and firn modeling, to detect melt in Antarctica, illustrating how SMRT can link microwave signals to firn state. Yet, the potential to directly constrain firn properties in densification models remains largely unexplored. Because grain size modulates the C-band backscatter, variations in grain size can obscure the backscatter–FAC relationship. Any backscatter-based FAC retrieval must therefore first account for grain-size variability.

Building on these earlier studies, we leverage 15 years (2007–2021) of ASCAT backscatter data to constrain an effective firn grain-size parameter across Antarctic ice shelves. By coupling IMAU-FDM with the SMRT model (referred to as FDM-SMRT coupling hereafter), we simulate radar backscatter and iteratively refine grain size estimates to minimize discrepancies with ASCAT observations. Beyond constraining grain size, this framework also allows us to examine how the sensitivity of ASCAT backscatter shifts across firn regimes and to evaluate how grain-size variability affects the interpretation of backscatter in terms of FAC. Specifically, we: i) assess the interannual variability of grain size and FAC and their respective relationships with ASCAT backscatter; ii) identify systematic biases in FDM-modeled grain size, particularly in regions influenced by

https://doi.org/10.5194/egusphere-2026-1263
Preprint. Discussion started: 7 April 2026

melt-refreezing processes; and iii) derive a more interpretable backscatter–FAC relationship by statistically reducing grain-size-driven scatter, as a proof of concept for potential FAC inference from ASCAT. The remainder of this paper is structured as follows: Section 2 describes the datasets used, including the ASCAT backscatter and IMAU-FDM simulations. Section 3 outlines the methodology, detailing the FDM-SMRT coupling framework, the sensitivity experiments, and the grain size optimization approach. Section 4 presents the results, comparing optimized and modeled grain size, evaluating the relationship between FAC and ASCAT backscatter, and analyzing the spatial distribution of firn properties across Antarctic ice shelves. Finally, Section 5 discusses the implications of our findings for firn modeling and ice shelf stability assessment.

2 Data

To assess firn properties across Antarctic ice shelves, we use a combination of active microwave satellite observations, firn model outputs, and optical remote sensing data for validation. Below, we describe each dataset, its relevance to this study, and the pre-processing steps applied.

2.1 C-band ASCAT Observations

The C-band Advanced Scatterometer (ASCAT) provides active microwave backscatter measurements that are highly sensitive to the firn microstructure, making it a valuable tool for assessing spatio-temporal variations in firn properties. ASCAT can penetrate several meters into the firn, allowing it to capture changes in grain size and FAC across ice shelves. For this study, we use vertically polarized data at a frequency of 5.255 GHz, obtained from the Brigham Young University Microwave Earth Remote Sensing Laboratory (Long et al., 1993). The data is expressed in the point-slope form, where the normalized radar cross section (σ_0, in dB space) measurement made by ASCAT is approximately a linear function of the incidence angle (θ_i)

$$\sigma_0(\theta_i) = A + B(\theta_i - \theta_{ref}) \tag{1}$$

where, θ_{ref} is reference angle (i.e. a mid-swath value of 40° for ASCAT), A measured in dB is the value of σ_0 normalized at 40° incidence angle, and B measured in $dB/^\circ$ describes the dependence of σ_0 on θ_i. The azimuth dependence of σ_0 is discarded in this dataset as the σ_0 values are largely azimuth-independent over most of the regions of the Earth (Long et al., 1993). As per equation 1, we use the A parameter for our analysis because after removing the incidence angle dependence, A is sensitive to depth-weighted near surface (i.e. ≈ upper 20 m) snow grain size (Fraser et al., 2016).

The original data have a resolution of 4.45 km, but are resampled to 27 km using a Nearest-Neighbor method to match the spatial resolution of IMAU-FDM. This resampling preserves the original backscatter signal without introducing interpolation artifacts. To minimize the influence of seasonal melt effects, we focus on winter (June, July, and August, or JJA) mean backscatter values for each year between 2007 and 2021, yielding 15 values per pixel for temporal analysis. Pixels of Antarctic ice shelves that experienced major calving (i.e., where Greene et al. (2022)'s annual calving-front outline indicates a retreat or advance crossing the 27 km grid cell boundary in any year) were excluded from all years of analysis.

https://doi.org/10.5194/egusphere-2026-1263
Preprint. Discussion started: 7 April 2026

2.2 Model Data

The IMAU Firn Densification Model (IMAU-FDM) is a semi-empirical 1D model that simulates the vertical evolution of firn layers under the influence of surface mass balance (SMB) processes (Veldhuijsen et al., 2024). It provides high-resolution estimates of key firn properties, including density, temperature, FAC, and grain size, making it a widely used tool for Antarctic firn studies. However, grain size evolution in IMAU-FDM is parameterized with simplified assumptions that do not explicitly account for refreezing-driven grain growth, leading to potential biases in melt-affected regions (Veldhuijsen et al., 2024). This limitation motivates the need for ASCAT-based optimization in our study.

We use IMAU-FDM v1.2AD, which explicitly models grain growth as a function of temperature but does not incorporate direct observational constraints (Veldhuijsen et al., 2024). The model is forced with three-hourly fields of surface temperature, wind speed, snowfall, sublimation, snowdrift erosion, and melt from RACMO2.3p2 regional climate model outputs, driven by ERA5 reanalysis (van Wessem et al., 2018). The horizontal resolution of 27 km is set by RACMO2.3p2's grid spacing. IMAU-FDM output is available at a 10-day temporal resolution and a 4 cm vertical resolution.

To drive our coupled FDM–SMRT backscatter simulations at the same temporal spacing, we therefore extract density, temperature, grain size, and liquid water content from IMAU-FDM at those 10-day timesteps. SMRT then uses these inputs to produce synthetic backscatter intensity time series (Refer to Method Sec. 3.2), from which we compute winter (JJA) means for each year (2007–2021), exactly as done with the ASCAT-derived backscatter values. This results in 15 FDM-SMRT winter mean backscatter values per pixel for comparison with ASCAT backscatter.

In addition, we derive Melt-over-Accumulation (MoA) from RACMO2.3p2 data as an independent metric of firn melt intensity. MoA is defined as the ratio of total liquid water production (melt + rainfall) to snow accumulation (snowfall – sublimation) (van Wessem et al., 2018, 2023) over the study period (2007–2021). This MoA parameter helps distinguish regions where firn depletion is driven by sustained meltwater production, providing insight into areas where ASCAT backscatter and FAC may be strongly affected by refreezing processes.

2.3 Sentinel-2 Melt Pond Volume

To assess the relationship between firn saturation and microwave backscatter, we use melt pond volume estimates derived from Sentinel-2 optical imagery. Melt pond formation serves as a sensitive indicator of firn depletion and ice-shelf weakening, since refreezing of ponded water creates impermeable ice lenses that promote hydrofracture (van Wessem et al., 2023). This dataset thus provides an indirect (but useful) validation metric for ASCAT-based firn assessments.

The melt pond dataset includes austral summer (December–February) estimates from 2015 to 2022. Sentinel-2 imagery is processed using an automated water classification algorithm (Moussavi et al., 2020), which identifies liquid water features based on spectral reflectance characteristics (van Wessem et al., 2023). To facilitate comparison with IMAU-FDM and ASCAT data, we aggregate melt pond volumes onto the RACMO2.3p2 grid.

https://doi.org/10.5194/egusphere-2026-1263
Preprint. Discussion started: 7 April 2026

3 Methods

This section describes the methodology used to optimize firn grain size estimates by integrating IMAU-FDM outputs with ASCAT backscatter via the Snow Microwave Radiative Transfer (SMRT) model. For this, we first establish a baseline by comparing winter-mean ASCAT backscatter (A) with IMAU-FDM FAC and grain size, and RACMO MoA, and we contrast this against Sentinel-2 melt-pond volumes to identify depleted firn regions (Sect. 3.1). Next, we outline the FDM–SMRT coupling framework for simulating C-band backscatter from IMAU-FDM firn profiles and use it to quantify the sensitivity of radar backscatter to grain size in varying firn conditions (from high FAC values of healthy firn to low FAC values of depleted firn) through targeted experiments (Sect. 3.2), which in turn motivates our core grain-size inversion: we couple FDM profiles to SMRT and iteratively optimize a single grain-size parameter to minimize misfit with observed backscatter (Sect. 3.3). We then perform a variance-partitioning ANOVA (Sect. 3.4) to decompose the interannual variance in ASCAT backscatter into the fractions explained by FAC, by grain size, by their interaction, and by residuals, thereby identifying the dominant driver(s) of backscatter variability and quantifying how much unexplained variance is reduced by our grain-size optimization. Finally, we demonstrate how FAC could be assessed once optimized grain size is accounted for (Sect. 3.5).

3.1 Comparison of IMAU-FDM/RACMO2 outputs with ASCAT Observations

To establish a baseline, we compare winter-mean ASCAT backscatter with IMAU-FDM FAC and grain size, and RACMO2 MoA. For each parameter, we compute the pixelwise long-term winter-mean value and generate scatterplot of ASCAT backscatter versus a) FAC, b) MoA, and c) Grain Size across Antarctic ice shelves, coloring points by Sentinel-2 melt-pond volume to highlight cells with persistent ponding, indicative of reduced pore space and higher saturation, versus cells with little or no pond signal. This baseline analysis identifies regions where modeled firn properties alone fail to capture observed backscatter variability, motivating the more detailed sensitivity and inversion experiments that follow.

3.2 Coupling IMAU-FDM to SMRT and targeted grain-size sensitivity

To evaluate how well IMAU-FDM–derived firn profiles reproduce observed radar returns and to set up our grain-size inversion, we couple the model outputs with the Snow Microwave Radiative Transfer (SMRT) model (Picard et al., 2018). In our configuration, the SMRT model represents the snowpack as a composite of multiple horizontally placed layers up to the penetration depth of the C-band radar signal ($\sim$ 20 m depth) and simulates the volume scattering coefficient at both horizontal and vertical polarizations (Picard et al., 2018). Since the incident wavelength of ASCAT is 5.70 cm, we avoid using the sub-wavelength layer thickness in SMRT (4 cm, the original layer thickness from IMAU-FDM output). Instead, we merge two layers from IMAU-FDM output to create 8 cm layers that are appropriate for the ASCAT signal. For this, we use the average to preserve the bulk microstructural properties of the two sub-layers (Picard et al., 2018). Each layer is then characterized by temperature, liquid water content, and snow microstructure. We do not prescribe a reflective basal substrate in SMRT; instead, we approximate a semi-infinite lower boundary by setting the deepest layer thickness to 1000 m, so no separate 'background' backscatter term is imposed (Picard et al., 2022b).

https://doi.org/10.5194/egusphere-2026-1263
Preprint. Discussion started: 7 April 2026

The representation of snow microstructure is critical in the SMRT model, as it directly influences the choice of formulation used to compute the backscatter (Picard et al., 2018). In our analysis, we use an exponential microstructure as it has only one parameter (in contrast to other representations), which makes it easier to optimize (Picard et al., 2018). This single parameter is correlation length (cl), defined as the surface-to-volume ratio of equivalent spheres (Mätzler, 2002), and has been shown to be empirically and theoretically linked with the modeled grain size (Picard et al., 2022b; Mätzler, 2002), by:

$$cl = 4(1 - \rho/\rho_{ice})/\rho_{ice} ssa \tag{2}$$

where ρ is density in kg m^{-3}, ρ_{ice} is density of ice in kg m^{-3}, and ssa is specific surface area described as a function of modeled grain radius r in mm, i.e., $3/\rho_{ice} r$ (van Dalum et al., 2022). Such a scheme reduces the number of parameters to be constrained, thereby avoiding an under-representation problem when comparing the FDM-SMRT coupled simulations with ASCAT observations and ultimately inferring the firn properties.

We employ the exponential microstructure with density, temperature, liquid water content, and layer thickness as input parameters derived from the FDM profile of all gridded points across the Antarctic ice shelf. We consider the FDM profiles for the JJA months during the period from 2007 to 2021, along with the C-band wavelength and a 40° incidence angle, which represent the ASCAT sensor configuration parameters in SMRT. For the electromagnetic (EM) model, we utilize the symmetrized version of the Strong-Contrast Expansion (SCE) theory from Picard et al. (2022a) under the non-local approximation (SymSCE). This choice is made to avoid the breakdown of the scattering formulation that often occurs in other theories for intermediate densities (450-550 kg m^{-3}) and high frequencies for coarse-grained snow (Picard et al., 2022a). The multi-layer radiative transfer equation in SMRT is solved using the discrete ordinate method (Picard et al., 2018).

Because grain size is one of the main sources of uncertainty in IMAU-FDM's microstructure (Veldhuijsen et al., 2024) and exerts a strong influence on C-band backscatter (Picard et al., 2022b), we perform a targeted grain-size sensitivity experiment. At the same time, ASCAT backscatter is also influenced by other aspects of firn structure, including density, layering, and ice saturation. However, the annual winter-mean ASCAT backscatter time series does not provide sufficient independent information to constrain all vertically varying firn properties simultaneously. We therefore prescribe firn stratigraphy from IMAU-FDM and treat grain size as the main unknown microstructural parameter.

To examine this sensitivity in representative firn regimes, we first select five 27 km cells spanning the range of FAC conditions, two 'healthy' (high FAC) sites on the Ross and Filchner-Ronne ice shelves, and three 'depleted' (low FAC) sites on the Amery, Larsen-B, and Baudouin blue-ice regions, to illustrate the sensitivity of backscatter to grain size. For each site, we extract the long-term (2007–2021) winter-mean firn profile from IMAU-FDM (density, temperature). The grain size is kept constant across all layers up to 20 m depth. This approach maintains consistency with our optimization scheme, where we estimate a single grain size value for the entire snowpack. We then systematically vary the grain size value from 0 to 10 mm (in 0.5 mm steps) and run the FDM–SMRT coupled model to simulate the winter-mean backscatter at each grain size. Ultimately, we quantify how backscatter responds to grain size in "healthy" versus "depleted" firn.

However, C-band backscatter is also sensitive to the firn's saturation state described by FAC; a grain–size–only experiment thus cannot capture variability arising from density/FAC effects. Moreover, because FAC is not a direct input to SMRT (whereas

https://doi.org/10.5194/egusphere-2026-1263
Preprint. Discussion started: 7 April 2026

density is), we include a complementary 2-D sensitivity that varies both density and grain size built from an IMAU-FDM firn column. From a single FDM profile, we take the time-mean layer thickness and temperature for the upper 20 m and hold these fixed. We then generate a grid of snowpacks by assigning a uniform density ρ (in the range of $10 - 910\ \mathrm{kg\,m^{-3}}$) along the column and a uniform grain size r (in the range of 0.01 - 1.2 mm) to all layers. For each (ρ, r) pair, we run SMRT with the ASCAT configuration to obtain the simulated backscatter and plot it as a contour heatmap. To link density to FAC in this controlled setting, we translate uniform density to its equivalent 20 m FAC (depth-integrated air content) using equation 4 in Ligtenberg et al. (2014). This design isolates how backscatter varies with grain size versus density/FAC under identical vertical geometry and thermal state, clarifying regimes where the backscatter is microstructure-dominated versus FAC-dominated.

3.3 Optimization of Grain Size

Because IMAU-FDM's grain-growth scheme is parameterized rather than directly constrained by observations (Veldhuijsen et al., 2024), its native grain-size output may not fully represent the effective microstructure seen by ASCAT. We therefore estimate an effective grain-size parameter for each 27 km cell by minimizing the mismatch between winter-mean FDM–SMRT simulations and ASCAT observations.

We run the FDM–SMRT coupled model for the JJA months of each year (2007-2021) to compute a winter-mean simulated backscatter A_{sim} per cell and year across Antarctic ice shelves, then compare it to the corresponding ASCAT winter mean A_{obs} via equation 3 to retrieve the optimized grain size. The resulting inversion is repeated for all 15 years to yield one optimized grain size per year. We use mean-squared error (MSE) as a minimization metric between simulation and observation:

$$\mathrm{MSE}(r) = \frac{1}{N_t} \sum_{t=2007}^{2021} \left[\bar{A}_{\mathrm{sim}}(r,t) - \bar{A}_{\mathrm{obs}}(t)\right]^2 \tag{3}$$

where $N_t = 15$ is the number of years (2007-2021), $\bar{A}_{\mathrm{sim}}(r,t)$ is the SMRT-simulated winter (JJA) mean backscatter for year t given grain size r, and $\bar{A}_{\mathrm{obs}}(t)$ is the corresponding observed ASCAT winter (JJA) mean backscatter for year t. We employ the Limited-memory Broyden–Fletcher–Goldfarb–Shanno (L-BFGS) algorithm, implemented through SciPy, because it efficiently solves the optimization problem without requiring explicit computation of the Hessian matrix (Virtanen et al., 2020). Given the computational expense of the optimization process, we utilize the DelftBlue supercomputer (Delft High Performance Computing Centre , DHPC), allocating 16 cores for each of the 2000 gridded points. Ultimately, the relationship between correlation length and grain size, from equation 2, is exploited to provide an estimate of grain size based on the optimized correlation length. Note that the inversion targets a single, column-wide (uniform-with-depth) grain-size parameter representative of the upper $\sim$20 m firn column sampled by ASCAT; it should therefore not be interpreted as a depth-resolved grain-size profile.

By repeating the optimization for each year from 2007 to 2021, we estimate the interannual variability of the optimized effective grain-size parameter, particularly in regions where melt and refreezing may alter firn microstructure through time. As part of our analysis, we examine the spatial variability in grain size regimes across regions with different firn conditions. We further compare the optimized grain size with the mean grain size of the upper 20 m in IMAU-FDM to evaluate how well IMAU-FDM estimates the grain size at the Antarctic-ice-shelf-wide scale.

https://doi.org/10.5194/egusphere-2026-1263
Preprint. Discussion started: 7 April 2026

Because IMAU-FDM's grain-growth parameterization is weakly constrained under ice-saturated conditions (Veldhuijsen et al., 2024), where refreezing dominates and pore space is exhausted, we perform a targeted sensitivity test on depleted firn, where the largest biases between modeled and optimized grain sizes are expected. Across Antarctic ice shelves, we select all the cells with FAC < 1.5 m (35 cells total), extract each cell's ice-saturation depth, and compute the grain-size difference ($\Delta r = r_{\mathrm{FDM}} - r_{\mathrm{opt}}$) for those cells. Here, ice saturation is a threshold concept: we define the ice-saturation depth as the shallowest depth at which the modeled firn density equals that of solid ice. This differs from FAC, which is a continuous, column-integrated air-volume metric derived from the vertical density profile. We then examine the relationship between Δr and ice-saturation depth to diagnose how deep versus shallow ice-saturation affects the grain size bias.

3.4 Explaining the interannual variability of ASCAT from firn properties

To examine how ASCAT backscatter varies with interannual changes in grain size and FAC, we perform an Analysis of Variance (ANOVA) using the annual profile of grain size and FAC (i.e., 15 values for the period 2007–2021). ANOVA allows us to decompose the total year-to-year variance in backscatter into the portions associated with FAC, grain size, and their interaction, thereby quantifying each factor's relative importance (Gelman, 2005). Because the optimized grain size is inferred by fitting FDM–SMRT simulations to ASCAT observations, the variance partitioning presented here should be interpreted as a conditional diagnostic within the adopted framework rather than as an independent attribution of ASCAT variability. In this sense, the ANOVA is used to examine how interannual ASCAT variability projects onto FAC and the optimized effective grain-size parameter within the assumptions of the inversion.

To examine how the explanatory power of FAC, grain size, and unexplained variance shifts across different firn saturation states, we group all 27 km cells into 50 quantile-based FAC bins (based on their long-term mean FAC). Within each bin, we compute the mean and interquartile range (IQR = Q75–Q25) of the ANOVA-derived fractions after optimization: the FAC main effect f_{FAC}, the grain-size main effect f_{r}, the interaction term $f_{\mathrm{FAC\times r}}$, and the unexplained fraction $f_{\mathrm{unexplained}} = 1 - (f_{\mathrm{FAC}} + f_{\mathrm{r}} + f_{\mathrm{FAC\times r}})$. We use the IQR because it robustly captures the central 50% of the bin-to-bin variability without being skewed by extreme outliers. We then normalize both the mean and the IQR of each component by the total mean variance in that bin, yielding fractional contributions and fractional IQRs that sum to unity. This normalization is purely statistical (a rescaling of variance fractions for comparability across FAC bins) and does not modify the underlying physical sensitivity of ASCAT backscatter. Finally, by plotting these binned statistics against the bin's average FAC, we identify the FAC regimes in which grain size or FAC has a larger role in explaining backscatter variability and quantify the uncertainty (via the IQR bands) associated with each component's explanatory power.

3.5 Assessment of the backscatter–FAC relationship after grain-size standardization

We explore a proof of concept for interpreting ASCAT backscatter in terms of FAC by standardizing grain size to reduce grain-size-induced spread in the backscatter-FAC relationship. First, we perform the physical inversion and retrieve an optimized grain size r_{opt} for each grid cell and year by minimizing the mismatch between FDM-SMRT-simulated and ASCAT-observed backscatter, given the IMAU-FDM stratigraphy (as in Sect. 3.3). We then apply a purely statistical post-processing step: using

https://doi.org/10.5194/egusphere-2026-1263
Preprint. Discussion started: 7 April 2026

all paired winter-mean $(\mathrm{FAC}, r_{\mathrm{opt}})$ values across Antarctic ice shelves, we fit a smooth cross-cell central tendency $r_{\mathrm{std}}(\mathrm{FAC})$ (represented by a power law fitted by ordinary least squares as the FAC–grain size relationship is non-linear (Veldhuijsen et al., 2024)). This fitted function assigns each FAC value a single 'standardized' grain size r_{std}, which we use only after inversion.

The motivation for this standardization is that C-band backscatter is highly sensitive to microstructure (grain size). Therefore, when examining backscatter as a function of FAC across many cells, inter-cell and interannual variations in grain size introduce additional spread even at a fixed FAC (i.e., 'grain-size-driven scatter'). By replacing r_{opt} with $r_{\mathrm{std}}(\mathrm{FAC})$, we treat grain-size variability as a nuisance source of scatter and obtain a more interpretable diagnostic backscatter-FAC curve that more directly reflects the FAC sensitivity. Importantly, $r_{\mathrm{std}}(\mathrm{FAC})$ is not used as a prior or constraint in the inversion and is not interpreted as a unique physical law relating FAC and grain size. Finally, we compare A_{std} values with FAC to evaluate the standardized backscatter–FAC relationship, i.e., after reducing the spread caused by inter-cell and interannual grain-size deviations.

4 Results

4.1 Comparison of ASCAT backscatter with IMAU-FDM/RACMO2 Outputs

Fig. 1 illustrates the relationship between ASCAT observations, IMAU-FDM FAC, grain size and MoA from RACMO2.3p2 across Antarctic ice shelves, alongside the S-2 integrated melt pond volume. In Fig. 1a, we observe large spatial variability in the winter mean ASCAT backscatter for the period from 2007 to 2021, with notably distinct spatial patterns recorded in ASCAT data (i.e. transition from low to high backscatter and vice versa) for the Amery, Ross, and Filchner-Ronne ice shelves. Fig. 1b reveals the characteristic inverted U-curve between winter-mean ASCAT backscatter and IMAU-FDM FAC (Alley et al., 2018), i.e., backscatter peaks at intermediate FAC and is lower at both low and high FAC. Fig. 1c shows the same pattern against RACMO2 MoA. In both panels, the Sentinel-2 melt pond volume is overlaid, which demonstrates a strong link with depleted firn conditions.

In regions with high FAC (which in general indicates a low MoA), the ASCAT backscatter is low because the snowpack consists of smaller grains, which remain transparent to the incoming radar signal. This transparency increases radar signal penetration and results in lower radar return values due to scattering losses in the snowpack. Conversely, as FAC decreases due to increased melt events, refreezing leads to larger grain sizes, thus increasing backscatter. However, in areas with low FAC, persistent melt can form thin refrozen ice lenses (typically < 10 cm thick) within the firn (Pfeffer et al., 1991). Although these lenses are density discontinuities, they behave like planar, specular reflectors: most of the radar energy is reflected away from the side-looking ASCAT antenna rather than back toward it. At the same time, the presence of one or two dominant ice layers suppresses the smaller-scale grain-boundary scatterers that normally drive diffuse volume backscatter, so the net result is a decrease in the measured radar return in regions of intense melt.

Such an inverted U-curve relationship can also be observed in Fig. 2 of Alley et al. (2018), which explores the connection between ASCAT backscatter and melt days in Antarctica. This finding strongly aligns with the behavior depicted in Fig. 1c of our study, wherein the ASCAT backscatter is compared with MoA. Fig. 1d extends this baseline by showing winter-mean backscatter as a function of IMAU-FDM–modeled grain size. Here we see that backscatter rises as grain size increases from

https://doi.org/10.5194/egusphere-2026-1263
Preprint. Discussion started: 7 April 2026

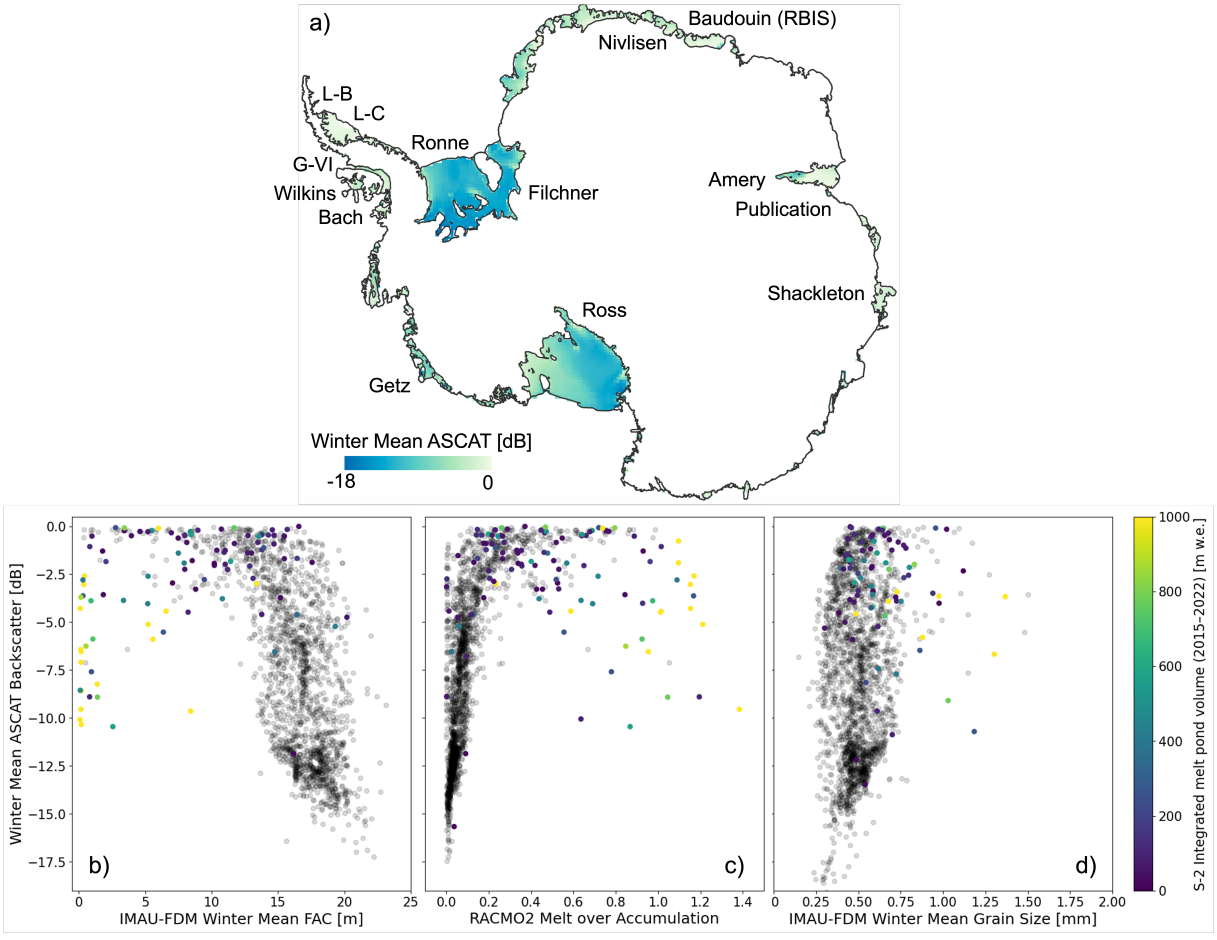

Figure 1. a) 2007 – 2021 winter mean ASCAT backscatter at the Antarctic-ice-shelf-wide scale. The relationship between winter mean ASCAT and b) IMAU-FDM FAC (i.e. inverted U-curve), c) RACMO2 Melt over Accumulation (MoA), and d) IMAU-FDM Grain Size with S-2 integrated melt pond volume in color whereas gray points are the regions with no S-2 melt pond data. G-VI is George-VI ice shelf, and L-B and L-C are Larsen-B and Larsen-C ice shelves respectively.

285 ≈ 0.2 mm up to ≈ 0.5 mm, where diffuse volume scattering is maximized, and then declines again for coarser grains as the number of grain-boundary interfaces per unit volume decreases and forward scattering/attenuation increases, which can dampen the C-band return (Picard et al., 2022a). Taken together, these baseline comparisons show that, although ASCAT backscatter is influenced by FAC and melt-pond signals, variations in grain size exert a strong first-order influence on C-band returns, highlighting the critical role of microstructural variability in driving the observed backscatter patterns.

https://doi.org/10.5194/egusphere-2026-1263
Preprint. Discussion started: 7 April 2026

4.2 Sensitivity of ASCAT backscatter to Grain Size in varying FAC regimes

Fig. 2 demonstrates how backscatter sensitivity to microstructural versus saturation controls varies across contrasting firn regimes. Fig. 2a shows the broad spatial variability in winter-mean FAC across Antarctic ice shelves, ranging from the deeply porous firn of Ross and Ronne ice shelves in West and East Antarctica, through intermediate conditions in the Baudouin blue-ice region, to the heavily depleted layers of Larsen-B and Amery ice shelves. To explore how these contrasting saturation states influence radar returns, we perform a sensitivity experiment (Fig. 2b) targeted to five 27 km grid cells, two "healthy" sites (Ross, Filchner–Ronne) and three "depleted" sites (Larsen-B, Amery, Baudouin), which are mapped in Fig. 2a. Because Larsen-B represents an important depleted-firn case in the Antarctic Peninsula, the selected grid cell was chosen to remain within the ice-shelf mask throughout the study period, excluding surrounding sea-ice-covered areas.

Across all sites, we notice that the FDM-SMRT simulated backscatter rises sharply as modeled grain size grows from near zero to about 1 mm, then plateaus for larger grains, demonstrating the classic volume scattering response of C-band waves (Picard et al., 2022b). Crucially, when we overplot the observed winter-mean ASCAT backscatter (dots) at each site's IMAU-FDM grain size, nearly all points fall on the steep portion of the curve rather than in the flat plateau. This steepness further depends on the firn condition (i.e., FAC value). In regions with high FAC, such as Ross and Ronne, the increase is relatively steeper compared to regions with low FAC. Note that the red (Ross) and yellow (Ronne) curves almost coincide because both sample dry regime (FAC $>$ 15 m), producing nearly identical backscatter signatures. For the samples situated on the slope of the curve, even small errors in the modeled grain radius translate into multi-decibel biases in in the FDM-SMRT simulated backscatter.

Conversely, as firn conditions deplete, some samples approach the shallow-slope ('plateau') part of the curve (e.g., Amery). In this regime, backscatter is less affected by variations in grain size; however, even a small change in FAC (e.g., from 0.69 m in Larsen-B black line to 0.11 m in Amery blue line) causes backscatter to drop from approximately 0 dB to around -5 dB. Thus, the five-site sensitivity test shows that ASCAT's grain-size leverage is strong on the steep limb, but weakens as shelves enter depleted (low FAC) conditions. To generalize this behavior beyond the five examples and make the density/FAC dimension explicit, we map the joint response $\sigma^0(\rho, r)$ in Fig. 2c. The 2-D surface shows that at intermediate densities (roughly $\rho \sim 200 - 700\ \mathrm{kg\,m^{-3}}$; mid-FAC for a 20 m column), backscatter varies most strongly with grain size: moving from small to moderate r produces large increases in σ^0, while changes in ρ within this band have comparatively modest effect. By contrast, at the low-density/high-FAC and high-density/low-FAC ends, the surface becomes flat in r and steeper in ρ, indicating that the response is increasingly governed by the ice-saturation state rather than microstructure. In practical terms, ASCAT offers strong leverage to constrain grain size in the mid-density regime, whereas at very low or very high densities/FAC the signal is primarily modulated by density/FAC and grain size becomes more weakly identifiable. Importantly, the fact that ASCAT is sensitive to grain size enables us to refine it, providing an opportunity to better constrain one of the main sources of uncertainty in IMAU-FDM's firn microstructure (Veldhuijsen et al., 2024) and thereby reduce biases in modeled grain size. In the next section, we do so by performing a full inversion of grain size against the winter-mean ASCAT backscatter.

https://doi.org/10.5194/egusphere-2026-1263
Preprint. Discussion started: 7 April 2026

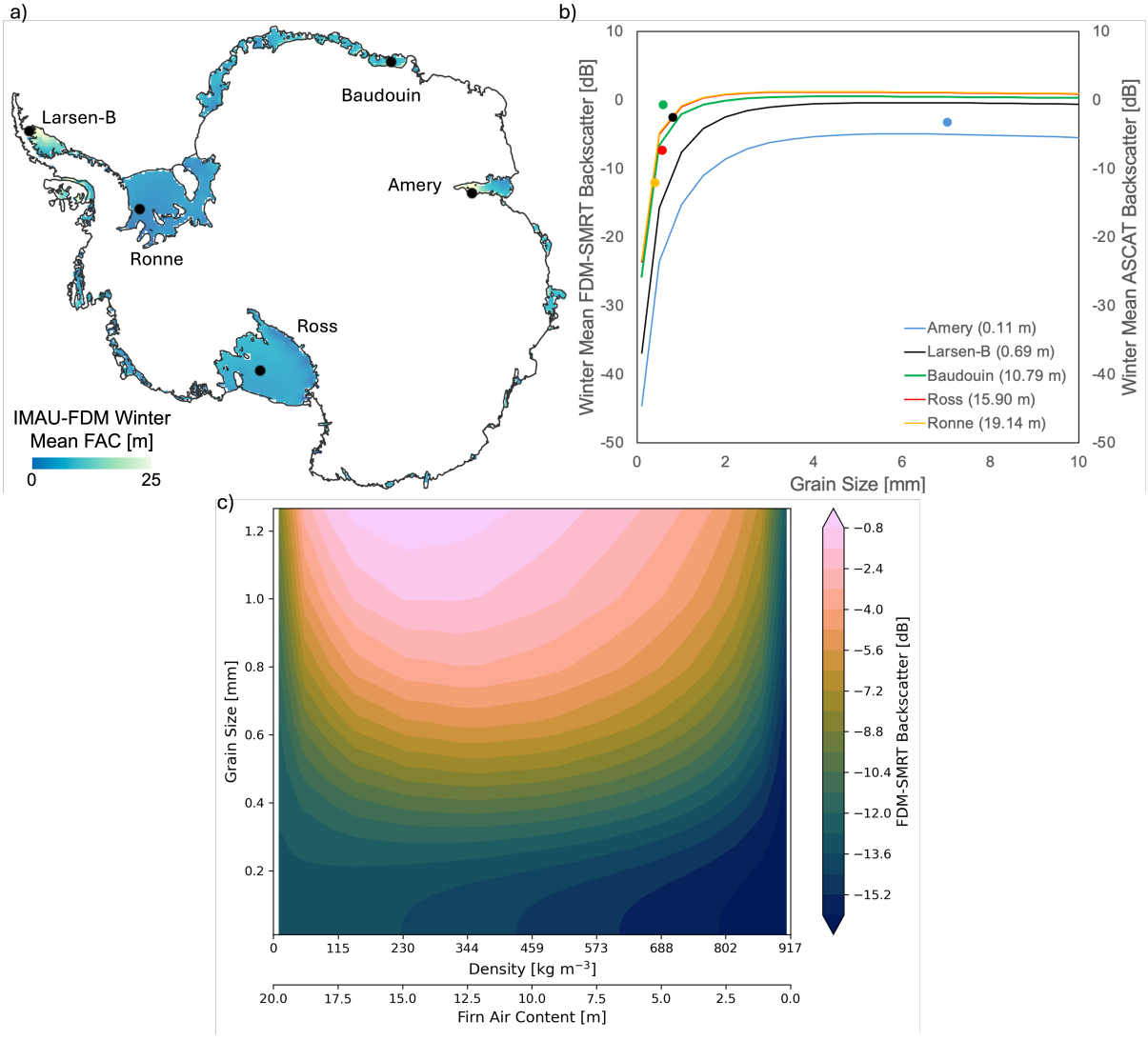

Figure 2. (a) 2007 – 2021 IMAU-FDM winter mean FAC at the Antarctic-ice-shelf-wide scale. Five samples are represented by black dots from Ross, Amery, Baudouin, Ronne, and Larsen-B ice shelves. b) Sensitivity of FDM-SMRT simulated backscatter to grain size for five samples, as shown by coloured lines. The coloured dots represent the observed winter mean ASCAT backscatter and IMAU-FDM grain size for the corresponding sample. In the legend, the winter mean FAC values from IMAU-FDM are noted in brackets for the respective locations. c) 2-D sensitivity of FDM-SMRT simulated backscatter in color to grain size and density/FAC.

4.3 Optimized grain size estimates at the Antarctic-ice-shelf-wide scale

Fig. 3 compares the mean grain size modeled from IMAU-FDM with the optimized grain size, using FDM-SMRT coupling and ASCAT observations, across the Antarctica ice shelves. The performance of the optimization between the FDM-SMRT

https://doi.org/10.5194/egusphere-2026-1263
Preprint. Discussion started: 7 April 2026

coupled simulations and ASCAT observations is illustrated in the Appendix (Fig. A1). The results indicate that the FDM-SMRT coupled model closely reproduces the ASCAT backscatter after optimization, achieving a correlation value close to 1 and root mean square error of 0.18 dB. Because the optimized grain size is inferred by fitting the model to ASCAT, this agreement should be interpreted as internal consistency within the adopted framework rather than as independent validation.

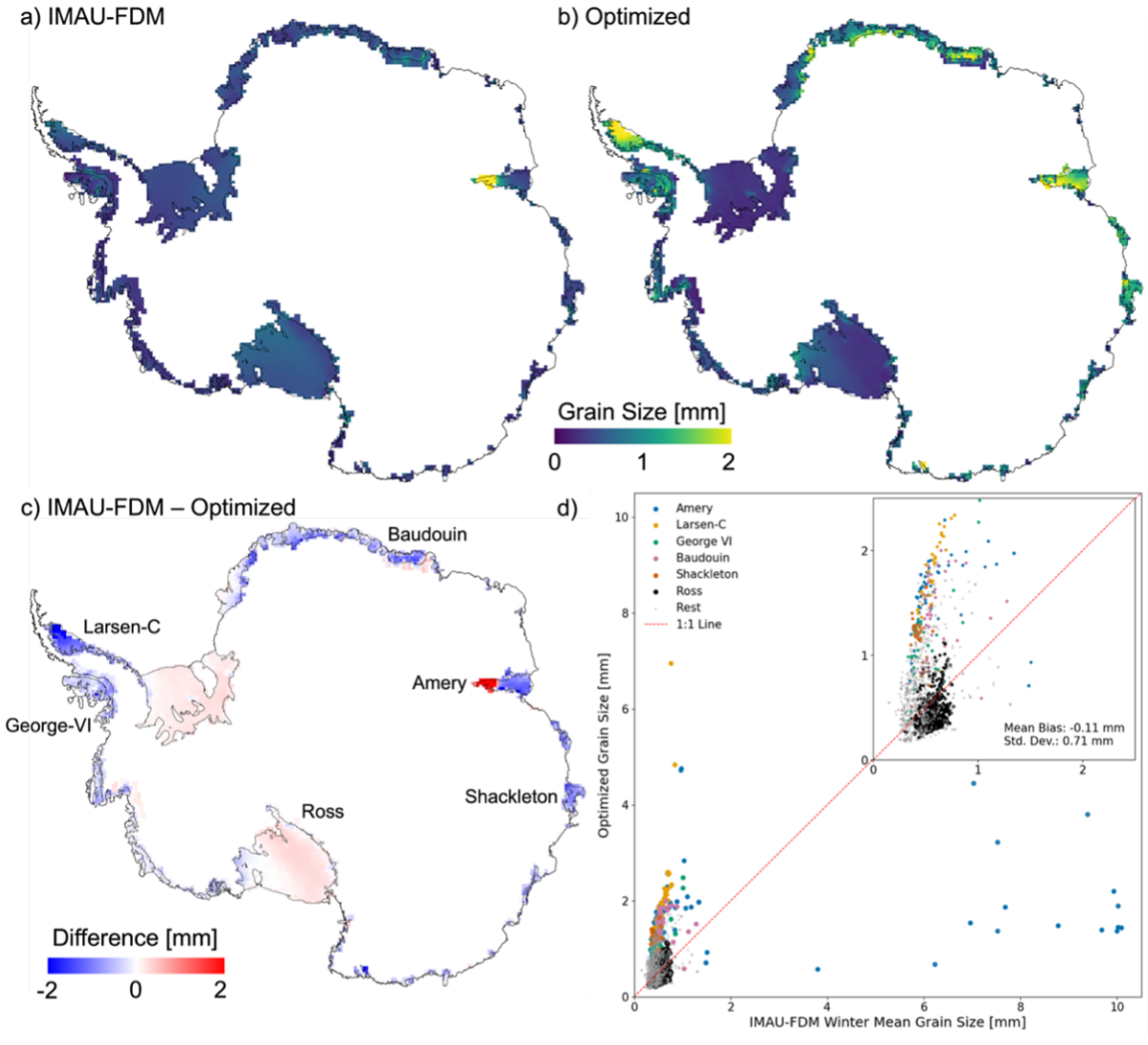

Figure 3. a) IMAU-FDM winter mean, b) Optimized, c) Difference (IMAU FDM - Optimized) grain size map, and d) Comparison between IMAU-FDM winter mean and Optimized grain size at AIS wide scale. Inset zooms the [2.5, 2.5] mm range where most of the points fall. The data points of all other ice shelves are categorized in "Rest" class, indicated by grey colour.

330 In Fig. 3a and b, we observe that IMAU-FDM tends to underestimate grain size in most regions compared to the optimized values. Large spatial variability in the optimized grain size is evident among East Antarctica, the Antarctic Peninsula, and West

https://doi.org/10.5194/egusphere-2026-1263
Preprint. Discussion started: 7 April 2026

Antarctica. Notably, we find much larger grain sizes in East Antarctica and the Antarctic Peninsula, regions characterized by substantial melt while falling in the intermediate to low FAC range of $\sim$ 5 - 10 m. In contrast, the average grain size in ice shelf regions of West Antarctica is relatively small. Although dynamic near-surface processes such as meltwater refreezing can lead to localized grain growth (Veldhuijsen et al., 2024), the high accumulation rates typical of West Antarctic ice shelves counteract long-term grain growth, resulting in smaller mean grain sizes compared to East Antarctica and the Antarctic Peninsula.

In Fig. 3c, ice-saturated areas near the grounding line of the Amery Ice Shelf exhibit severely overestimated grain sizes in IMAU-FDM, with differences of approximately 8 mm (highlighted in red). In contrast, a sharp transition is observed in Amery for the relatively dryer and colder regions towards the coast, wherein severe underestimations of grain size by IMAU-FDM are observed. This observation is also made in Larsen-C ice shelf. For dry ice shelves, such as the Ross and Ronne Ice Shelves, the grain sizes from IMAU-FDM closely align with the optimized values, falling near the 1:1 line (Fig. 3d); however, the model still slightly overestimates the grain size. The refreezing of meltwater impacts the snow structure by increasing grain size; however, IMAU-FDM has a limited response to this effect. The model assumes quite a small refreezing grain size of 0.25 mm (van Dalum et al., 2022), primarily affecting only the top surface of the firn (Veldhuijsen et al., 2024).

In Fig. 3d, we observe an overall mean bias in grain size of -0.11 mm relative to the 1:1 line, with a standard deviation of 0.71 mm. This large standard deviation is due to significant underestimations in the depleted regions of Larsen-C ice shelf and overestimations in the depleted regions of Amery ice shelf, where these points can be considered outliers, deviating markedly from the 1:1 line.

In order to understand these varying results, we relate the difference between IMAU-FDM modeled and optimized grain size for depleted regions with the ice-saturation of the firn layer, as in Fig. 4. It is evident that regions of the Amery ice shelf, where the entire firn column is ice-saturated from the near-surface (i.e., at a depth of $<$ 2 m), show severely overestimated grain sizes in IMAU-FDM. This is indicated by large difference in grain size, i.e. 2–8 mm (refer to Fig. 3c). However, as this depth increases, the grain size shifts toward pronounced underestimation, particularly in the Larsen-C region. Meanwhile, at the transition, several locations with intermediate ice-saturation depths (including Shackleton, Wilkins, George-VI, remnants of Larsen-B) and ice shelves in East Antarctica (e.g., Publications) exhibit well-matched grain sizes. Moreover, at deep saturation depths, most ice shelves (Larsen-B, George-VI, Wilkins) also remain close to the 1:1 line. The exception is a small cluster of five points on Larsen-C, where IMAU-FDM underestimates grain size by several millimeters. These results highlight that while IMAU-FDM can perform well under specific conditions, its performance is highly dependent on the degree of ice saturation and the associated firn processes.

4.4 Explained variance in ASCAT backscatter from FAC and Grain Size

Fig. 5 synthesizes the contributions of grain size (GS), FAC, their interaction (FAC×GS), and unexplained variance to the ASCAT backscatter signal as a function of mean FAC. This plot highlights the shifting importance of grain size and FAC across different FAC regimes (see Appendix Fig. B1 for the spatial distribution of the contributions).

In regions with high FAC (e.g., $>$ 10 m), the ASCAT signal is associated primarily with grain size within the adopted framework, with the blue fraction peaking and narrow IQR bands indicating relatively consistent behavior across cells (Fig.

https://doi.org/10.5194/egusphere-2026-1263
Preprint. Discussion started: 7 April 2026

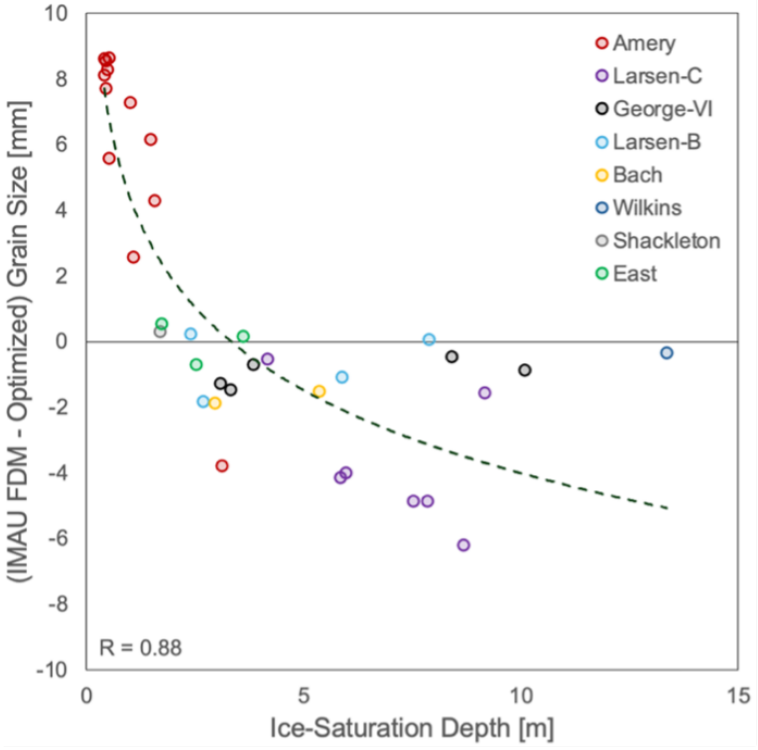

Figure 4. Relationship between (IMAU-FDM minus Optimized) grain size and the depth after which the firn column becomes ice for depleted regions at the Antarctic-ice-shelf-wide scale. East consists of ice shelves in East Antarctica, i.e. Publications and two unnamed ice shelves. The black dashed line shows the best-fit curve and R is the Pearson correlation coefficient. Here, all the data points fall in depleted firn regime (FAC $<$ 1.5 m).

5a). Here, the firn is more porous and is less frequently affected by melt-driven ice layers or saturation. These IQR trends also remain consistent for the unexplained contribution, suggesting that the dominant contributors to ASCAT variability (FAC and grain size) are better captured by the model in regions with FAC values $>$ 10 m, leaving fewer unexplained factors.

As FAC falls below $\approx$ 10 m, the red FAC contribution rises sharply while the grain-size fraction declines, marking the transition toward firn-saturated conditions where density controls backscatter. The FAC$\times$GS interaction term is consistently small relative to the main effects across FAC regimes, indicating that most explainable variance is captured by the additive main effects of FAC and grain size rather than by their interaction. In low-FAC regions, the firn is highly heterogeneous due to processes such as temperature-driven metamorphism, refreezing, and ice saturation. These regions thus experience larger variability in both FAC and grain size contributions to ASCAT backscatter, amplifying cell-to-cell scatter in each component's contribution (high IQR). Finally, when plotting the ASCAT variance in Fig. 5b, we find it is stable in high-FAC regions but increases slightly in low-FAC regions, reflecting heightened interannual backscatter variability under saturated firn. These aggregated curves show how the relative roles of grain size and FAC shift systematically with FAC.

https://doi.org/10.5194/egusphere-2026-1263
Preprint. Discussion started: 7 April 2026

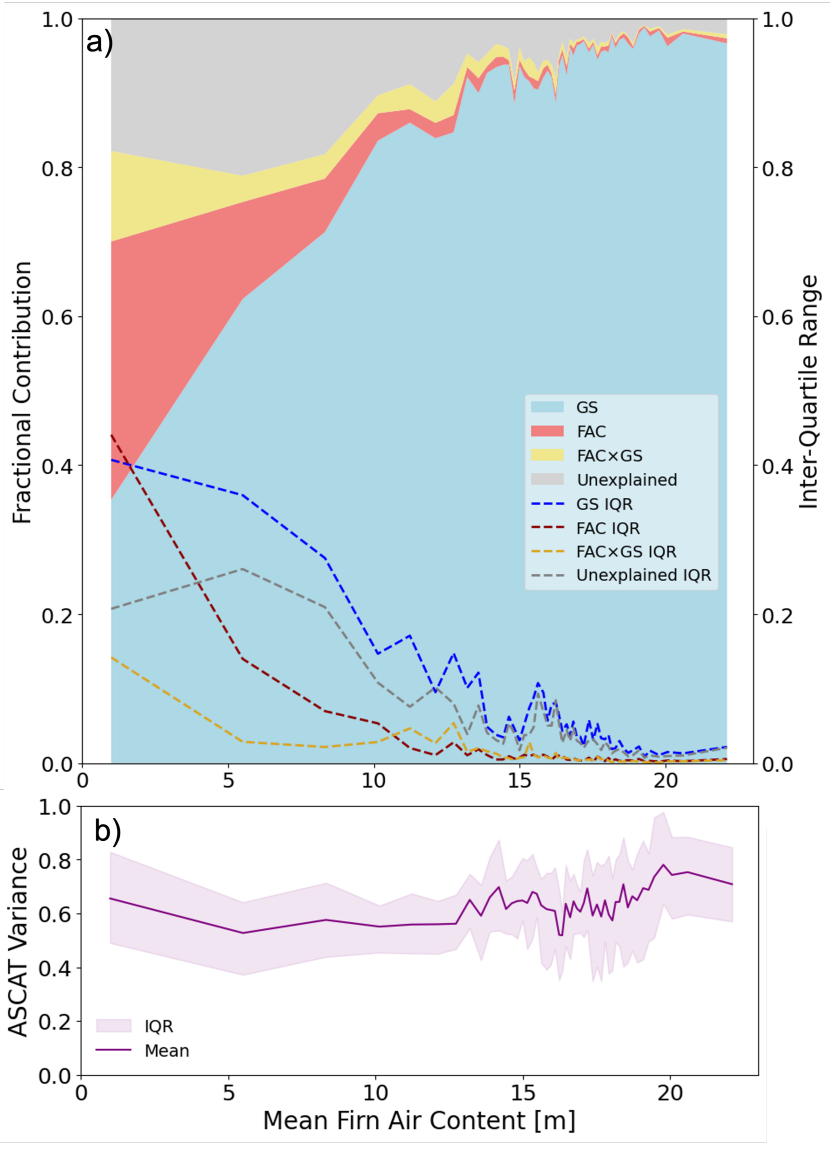

Figure 5. a) Fractional contribution of interannual ASCAT backscatter associated with grain size, FAC, their interaction (FAC×GS), and the unexplained component, with uncertainty represented by the IQR. b) Mean ASCAT variance in dB as a function of mean FAC.

4.5 Assessing FAC from ASCAT observations after grain size correction

Fig. 6 presents the relationship between FDM-SMRT simulated ASCAT backscatter and IMAU-FDM winter mean FAC under two conditions: (a) with optimized grain size, and (b) with standardized grain size extracted from a power law fit on the FAC – optimized grain size relationship (see Appendix Fig. C1b). This comparison illustrates how grain-size variability affects the interpretability of the backscatter–FAC relationship.

https://doi.org/10.5194/egusphere-2026-1263
Preprint. Discussion started: 7 April 2026

In Fig. 6a, where the grain size effect is included, we observe significant variability in the backscatter values for a given FAC. This variability confirms the influence of both FAC and grain size on backscatter (Alley et al., 2018; Picard et al., 2022b). In contrast, Fig. 6b, where the grain-size effect has been statistically standardized, shows a more coherent relationship between backscatter and FAC, resembling a smoother inverted U-curve. As already seen in Fig. 1, this adapted curve also indicates that backscatter is low in high-FAC ($>$ 15 m) firn, rises linearly to a maximum near FAC $\approx$ 1.5 m, and then declines sharply for FAC $<$ 1.5 m as the snowpack becomes depleted and dominated by dense ice layers. The key insight is that once the grain-size-driven scatter is reduced, the relationship between backscatter and FAC becomes more coherent and easier to interpret. This suggests that a substantial part of the spread in Fig. 6a is associated with grain-size variability, and that standardizing grain size makes the backscatter–FAC relationship more interpretable.

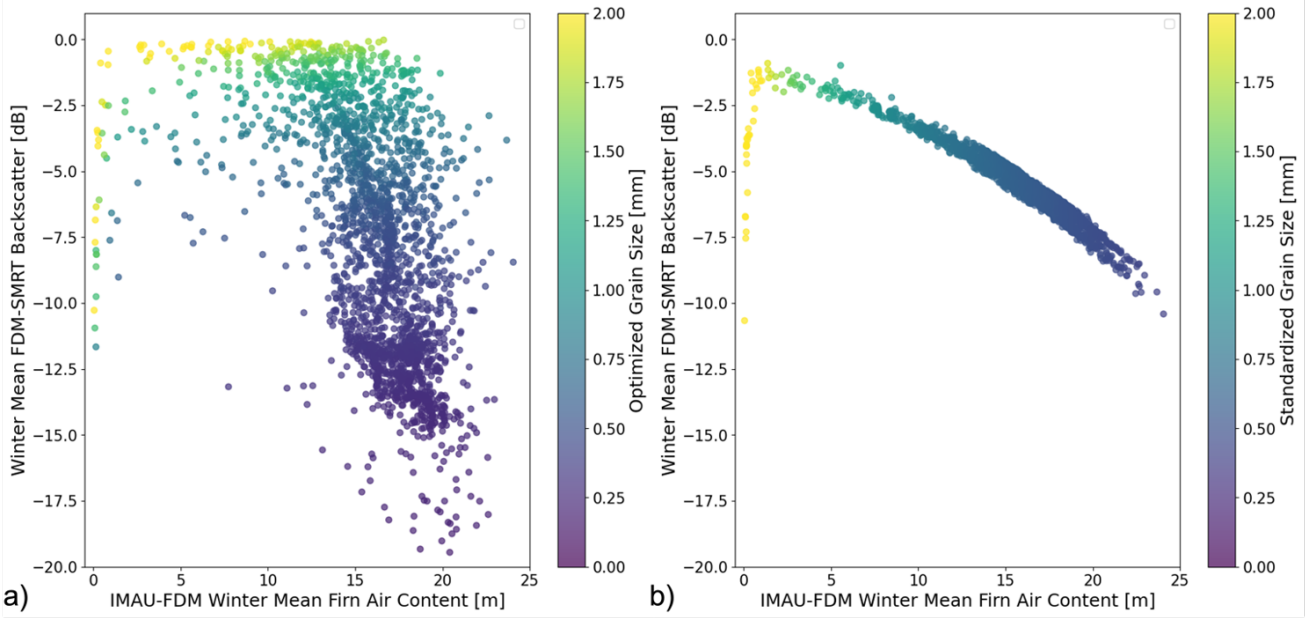

Figure 6. a) Inverted U-curve with grain size variations and b) Adapted inverted U-curve without grain size variations at the Antarctic-ice-shelf-wide scale.

5 Discussion

Our analysis demonstrates the comprehensive use of ASCAT observations to improve our understanding of firn properties, specifically grain size and FAC, on an Antarctic-ice-shelf-wide scale. Methodologically, we follow the same principle of coupling a firn model (IMAU-FDM) with a radiative transfer model (SMRT) to interpret microwave signals and optimize the grain size, as also explored by Dattler et al. (2024). However, our approach differs in scope and objective: (a) we use active C-band ASCAT backscatter, whereas Dattler et al. (2024) used passive AMSR-2 brightness temperatures for physics-based

https://doi.org/10.5194/egusphere-2026-1263
Preprint. Discussion started: 7 April 2026

melt detection; and (b) we perform an ice-shelf-wide, per-pixel, per-year inversion to optimize grain size, whereas Dattler et al. (2024)'s study was limited to 13 sites and Larsen-C ice shelf. Beyond these differences, our study brings three contributions. First, it delivers a scaled-up, ASCAT-constrained grain-size product with ice-shelf-wide coverage and annual cadence. Second, we apply variance-partitioning ANOVA to quantify how interannual backscatter variability is apportioned between grain size and FAC and to diagnose residual structure. Because the optimized grain size is itself inferred from ASCAT through the FDM-SMRT inversion, these post-optimization analyses are interpreted as conditional diagnostics within the adopted framework rather than as independent confirmation of process attribution. Third, by standardizing grain size, we derive an adapted backscatter–FAC relation indicating how FAC could be assessed from ASCAT, offering a potential pathway for large-scale firn monitoring. To support these results, we perform targeted 1-D/2-D sensitivity experiments (grain size and density/FAC) that delineate where ASCAT is microstructure- versus ice-saturation-dominated and provide a forward-model rationale for when grain size is identifiable.

Turning to the spatial patterns that emerge from this framework, we find that regions with high FAC exhibit low optimized grain size values (approximately < 0.5 mm), which aligns with the low grain size modeled by IMAU-FDM. Overall, we find that IMAU-FDM generally models smaller grain sizes compared to the optimized case; however, the severely depleted firn layer in Amery shows significantly larger grains. We attribute this variability in grain size estimates from IMAU-FDM to two primary factors: (a) the minimal effect of refreezing on grain size in IMAU-FDM and (b) a lack of calibration in depleted conditions. The grain growth model used in IMAU-FDM assumes that refreezing impacts grain size only if grain sizes are below 0.25 mm (Veldhuijsen et al., 2024). Consequently, for refrozen layers where the grain size exceeds 0.25 mm, the effect of refreezing on grain size becomes absent. Physically, meltwater refreezing can form ice lenses and melt-refreeze crusts with a coarser effective microstructure than dry-snow grains. The 0.25 mm threshold in IMAU-FDM is therefore not a physical upper limit on grain growth, but a simplifying parameterization that limits refreezing-driven coarsening once grains exceed this value. This explains the smaller grain size in IMAU-FDM compared to the optimized results across the Antarctic-ice-shelf-wide scale (as in Fig. 3c), suggesting that refrozen layers may have larger grain sizes than those represented in IMAU-FDM. One such example is the depleted region of Larsen-C, where we witness severe underestimation of grain size by IMAU-FDM. By contrast, Amery's depleted firn, despite its refrozen character, IMAU-FDM severely overestimates the grain size, yielding much larger grains compared to optimized results.

We explain these contrasting biases by the age of the firn-ice transition, which refers to the time it takes for firn to transform into glacial ice at a given location depending on factors such as accumulation rates, surface temperature, and densification processes (Veldhuijsen et al., 2023). In regions with an older firn-ice transition, such as the Amery Ice Shelf (1–1.5 kyr), the grains continue to grow indefinitely over time in the model based on temperature, as there is no prescribed maximum grain size in IMAU-FDM (Veldhuijsen et al., 2024). This leads to the formation of large grains, resulting in severe overestimation (Fig. 4d of Veldhuijsen et al. (2023)). Consequently, we infer that either the parameterization in IMAU-FDM is poorly constrained for such an old ice in Amery's depleted regions, where ice saturation begins at the near surface (Veldhuijsen et al., 2023), or the age of the ice itself may be not correct. In contrast, at the Larsen-C Ice Shelf, where the firn-ice transition is much younger (0.05–0.1 kyr), the limited time available for temperature-driven grain metamorphism yields inherently smaller modeled grains,

https://doi.org/10.5194/egusphere-2026-1263
Preprint. Discussion started: 7 April 2026

causing IMAU-FDM to underestimate the grain sizes. We thus anticipate that additional calibration data from these depleted regions will improve the accuracy of grain size estimates in IMAU-FDM.

Direct in-situ validation of grain size at the spatial support and vertical sensitivity of ASCAT is limited. Accordingly, the present results should be interpreted primarily as an internally consistent, ASCAT-conditioned effective parameterization rather than as a comprehensively validated external grain-size retrieval. In addition, IMAU-FDM has been evaluated primarily against available in-situ firn observations from Antarctica that are concentrated in non-melt (dry-snow) regions; model performance and calibration are best constrained under dry-snow conditions (Veldhuijsen et al., 2024). Consistent with this, we find that in predominantly dry-snow ice-shelf regions (e.g., Ross and Filchner-Ronne), the ASCAT-retrieved effective grain size closely matches the IMAU-FDM grain-size estimates (Fig. 3c), providing an internal consistency check in regimes where the model is best constrained. Where limited field observations are available, we additionally compared our retrieved effective grain size to in-situ grain-size measurements reported at sites D5 and D17, in the vicinity of the French station of Dumont d'Urville in Adélie Land, East Antarctica, for austral summers 2017-2021 (Arioli et al., 2023). Both sites fall within a single 27 km IMAU-FDM grid cell used in our analysis. For that cell, the mean IMAU-FDM grain size is 1 mm and the mean ASCAT-retrieved grain size is 0.56 mm, while the reported in-situ mean grain sizes are 0.55 mm (D5) and 0.43 mm (D17). Given the mismatch in seasonality (summer sampling versus our winter JJA means) and spatial scales (point measurements versus a 27 km grid-cell effective value), we treat this comparison as a plausibility check rather than a strict validation. Nevertheless, the retrieved estimate is closer to the in-situ magnitude than the unadjusted IMAU-FDM value, suggesting that the inversion moves the effective grain size toward field-observed values.

In regions with significant depletion near the grounding line of the Antarctic Peninsula, the Amery ice shelf, and blue ice areas of the Baudouin and Nivlisen ice shelves, our optimized grain size map shows larger grains. The spatial patterns observed in our study align strongly with the vulnerable regions identified across the Antarctic ice shelves in previous studies (van Wessem et al., 2023; Alley et al., 2018). These vulnerable regions have been characterized based on either analyzing how much warming is required for a particular ice shelf to reach the MoA limit of 0.7 (van Wessem et al., 2023) or understanding the link between melt days and ASCAT backscatter (Alley et al., 2018). As the ASCAT record continues to lengthen, our study provides a tool to monitor long-term changes in firn properties, particularly through optimized grain size. Such tools are essential for assessing the degree of ice-saturation in the firn and identifying regions susceptible to potential meltwater ponding, which are precursors to structural weakening and hydrofracture (Kuipers Munneke et al., 2014).

By exploiting the relationship between FAC and optimized grain size, our adapted inverted U-curve demonstrates the potential of using ASCAT backscatter to inform FAC inferences once grain-size effects are controlled (Fig. 6). At present, we regard this as an indicative proof of concept rather than an operational FAC retrieval curve. It remains conditioned on the adopted FDM-SMRT framework, the statistical standardization of grain size, and the assumptions used to distinguish firn regimes. Additional validation and treatment of ambiguities would be required before such a relationship could be used for standalone FAC retrieval. Converting observed backscatter to FAC will require (a) a rigorously validated calibration from observed to standardized backscatter, (b) explicit handling of the two-branch ambiguity at low returns with independent priors, and (c) representation of surface-scattering processes in dry, high-FAC regimes. For (a), a calibration step is required because the adapted

https://doi.org/10.5194/egusphere-2026-1263
Preprint. Discussion started: 7 April 2026

curve is defined in the standardized backscatter domain, whereas ASCAT provides observed backscatter that still contains grain-size, surface roughness, and other scene-dependent influences. For (b), where the mapping is locally monotonic, the FAC estimate is single-valued and direct. At low observed backscatter, however, the inverted-U shape yields two plausible states: a depleted, low-FAC branch and a dry, high-FAC branch. In these ambiguous cases, the branch can be selected with simple, independent priors (e.g., melt-pond presence from optical imagery, MoA climatology, field-based grain size where available) or guidance from firn models. Once the depleted- versus dry-side branch is identified, FAC can be read consistently from the adapted curve. For (c), unmodeled surface processes (roughness, snowdrift, accumulation variability) can shift ASCAT independently of grain size or FAC; we briefly flag the issue here and treat it in detail under Limitations below. These steps are beyond the scope of this study, but our results outline how such an assessment could be developed and evaluated.

5.1 Limitations and Future Scope

There are several limitations to this approach that warrant consideration. We do not provide formal posterior uncertainty estimates for the optimized grain size; instead, interpretive confidence is assessed from the forward sensitivity experiments, the regime dependence of identifiability, the unexplained ANOVA fraction, and the limited plausibility checks against available field observations. With this in mind, a first limitation concerns identifiability of grain size in the shallow-slope ("plateau") regime of the backscatter response (Fig. 2b-c). As shown by our sensitivity analysis, once the σ^0–r curve flattens (small $\partial\sigma^0/\partial r$), ASCAT provides limited leverage to refine grain size from a single C-band observation. This flattening occurs (i) at very large grains and (ii) in depleted firn (FAC ~ 0), where the 2-D response surface becomes nearly flat in r and comparatively steeper in ρ, indicating that changes in backscatter are governed more by density/FAC than by microstructure in this regime. The Amery case demonstrates the plateau regime but cannot be taken as representative of all such settings; broader sampling is needed. Accordingly, we avoid generalizing beyond the observed range and emphasize FAC interpretations where the response to r is weak. Future extensions that add frequency or incidence-angle diversity (or additional plateau-regime sites) should help tighten r constraints where the C-band response is flat.

A second consideration is variance attribution after inversion. By construction, the optimized grain size is obtained by fitting FDM-SMRT coupled simulations to ASCAT observations year by year; it is therefore expected that post-optimization ANOVA shifts variance from FAC or the residual to r_{opt} where the response is steep in r (Fig. 2). Our 2-D sensitivity surface supports this interpretation: at intermediate densities the surface is steep in grain size and comparatively flat in density, so interannual ASCAT variability should project primarily onto r, precisely where ANOVA assigns a larger fraction to r_{opt}. Conversely, at low- and high-density extremes (very high or very low FAC) the surface flattens in r and steepens in ρ, implying that variability should project more onto FAC; ANOVA indeed shows higher FAC contributions in the low-FAC regime. At the very high-FAC end, however, some dry shelves exhibit elevated unexplained variance, which we attribute to unmodeled surface-process controls (e.g., roughness, snowdrift, accumulation variability) that can modulate ASCAT independently of r or FAC (Fraser et al., 2016). In short, the variance reallocation after inversion follows the forward-model sensitivity, while the residual in dry, high-FAC zones points to missing surface physics.

https://doi.org/10.5194/egusphere-2026-1263
Preprint. Discussion started: 7 April 2026

Addressing this residual requires explicit treatment of surface processes rather than reinterpreting them as microstructure or FAC. We did not include this in our framework as the interplay among accumulation, erosion, and roughness complicates the interpretation of backscatter changes (Shukla et al., 2024). Concretely, we propose two steps for incorporating these effects into our optimization scheme. First, we will obtain independent constraints on surface roughness and drift/accumulation patterns (e.g., in-situ roughness surveys (Shukla et al., 2024), azimuthal anisotropy proxies for sastrugi and microtopography (Cartwright et al., 2022), and snow-transport constancy diagnostics (Poizat et al., 2024)) to validate how backscatter responds to surface conditions. Second, we will incorporate rough-surface scattering in the forward model by activating the SMRT surface module (Picard et al., 2018) and combining it with volume scattering under ASCAT geometry. With these additions, the total simulated backscatter (surface + volume) can be matched to ASCAT, potentially reducing unexplained variance in dry, high–FAC regimes and yielding a more faithful optimization of grain size.

Another limitation of our approach is the assumption of a constant grain size across all layers up to 20 m depth during optimization. This approach is adopted to avoid under-representation in the inversion problem due to the large number of unknowns (i.e., grain size and density/FAC for each layer) that must be inferred from a single backscatter measurement, an issue that has also caused optimizer collapse in previous multi-layer retrieval attempts (Charrois et al., 2016; Cluzet et al., 2020). By simplifying the optimization to a single representative grain size, we effectively prevent model instability and under-representation, especially across large spatial scales. Our approach allowed for the production of a stable and consistent grain size estimate across the Antarctic ice shelves, capturing broad spatial trends effectively.

However, this simplification contrasts with findings by Brucker et al. (2010), which demonstrate that grain size varies significantly with depth, thereby influencing the microwave scattering and absorption from layers with larger grains. Their findings also highlight the importance of accounting for depth-dependent grain size to accurately model microwave interactions with snow, which could refine the representation of firn microstructure in radiative transfer models (Brucker et al., 2010). As a next step, we foresee adopting a depth-resolved grain size model that accounts for expected vertical heterogeneity while minimizing computational challenges. This could be enabled by expanding the observation space with multi-sensor, multi-frequency constraints, i.e., integrating passive microwave (AMSR-2, SMOS) and SAR (Sentinel-1) data, and, looking ahead, incorporating forthcoming L-band missions (ROSE-L, NISAR) and P-band BIOMASS mission to extend penetration depth. Together, these datasets can be fused in a joint inversion framework (across frequency and incidence angle) to better resolve vertical grain-size heterogeneity more robustly. Alternatively, advanced optimization methods like Bayesian optimization (Pan et al., 2017) or genetic algorithms (Tedesco and Kim, 2006) could efficiently search for the optimal depth-varying grain size profile, reducing computational costs and improving the accuracy of FDM-SMRT coupling.

In the future, improved spatial resolution surface mass balance (SMB) products from RACMO at 2 km (Noël et al., 2023) could be utilized to simulate firn profiles from IMAU-FDM with enhanced resolution. This would be invaluable for our analysis, allowing for a more detailed understanding of changes in firn properties based on ASCAT observations. Ultimately, we envision the potential use of optimized grain size by the firn modeling community to constrain grain size parameters in their models. This could be achieved by integrating optimized grain sizes into the model parameterization process, thereby improving the representation of refreezing, snow compaction, and metamorphism processes that directly influence grain size.

https://doi.org/10.5194/egusphere-2026-1263
Preprint. Discussion started: 7 April 2026

6 Conclusions

In this study, we focused on utilizing ASCAT observations to evaluate firn properties, specifically FAC and grain size, modeled from IMAU-FDM on an Antarctic-ice-shelf-wide scale for the period from 2007 to 2021. We present a new estimate of grain size derived from optimizing the differences between FDM-SMRT coupled simulations and ASCAT observations. Our findings reveal significant spatial variability in optimized grain size compared to the estimates from IMAU-FDM. In regions with a dry snowpack, the optimized estimates closely align with the model predictions. However, as FAC decreases, many regions experience an underestimation of grain size by IMAU-FDM. In depleted areas with low FAC, the discrepancy between model and optimized estimates is largely influenced by the degree of ice saturation within the firn column. For instance, in the depleted region of Amery, IMAU-FDM significantly overestimates grain size, as the firn column is entirely ice, starting from a near-surface depth of 0.4 m. This leads to larger grain sizes in the model because it lacks a maximum grain size constraint, i.e. grain growth is not bounded by an upper limit, so grains can grow unrealistically large over long firn–ice transition ages. Conversely, in areas where the depth of complete ice saturation increases, such as Larsen-C, the model underestimates grain size. This is due to the refreezing scheme in the model, which inhibits grain growth when sizes exceed 0.25 mm. We find that, within the adopted framework, C-band backscatter is most sensitive to grain size in several firn regimes, and that the backscatter–FAC relationship becomes more interpretable once grain-size effects are reduced. This provides a proof of concept for how ASCAT observations could contribute to FAC-oriented firn monitoring once grain-size effects are accounted for. Moreover, by assessing the individual contribution of grain size and FAC on ASCAT variance, we found that: a) dry ice shelves, such as Ross and Filchner-Ronne, show enhanced sensitivity of backscatter to grain size variations, whereas b) the backscatter variability is strongly controlled by FAC variations in depleted ice shelf regions of Amery, George-VI, and Larsen-C. The optimized grain size should therefore be interpreted as an effective, ASCAT-conditioned parameter whose confidence is regime-dependent and whose independent validation remains limited. In this regard, our findings suggest that ASCAT observations provide a complementary monitoring metric for shifts in firn conditions that are relevant to stability of Antarctic ice shelves. Furthermore, our study opens new avenues for improving firn model parameterization and for using ASCAT observations to better diagnose the state of the firn layer.

Code and data availability. The C-band ASCAT data are available from the BYU Scatterometer Climate Record Pathfinder (https://www.scp.byu.edu/data/Ascat/SIR/Ascat_sir.html; Long et al., 1993). The Sentinel-2 melt pond volume dataset is available on Zenodo (https://zenodo.org/records/7334047; van Wessem et al., 2022). The code of IMAU-FDM v1.2AD is available on Zenodo (https://doi.org/10.5281/zenodo.10723570; Veldhuijsen, 2024). The continent-wide IMAU-FDM profiles and the optimized grain-size dataset produced in this study can be obtained from the authors upon request.

https://doi.org/10.5194/egusphere-2026-1263
Preprint. Discussion started: 7 April 2026

Appendix A: FDM-SMRT Coupled Simulation vs ASCAT Observation

Fig. A1 shows the performance of FDM-SMRT coupling upon optimization, when compared with the ASCAT observations for all the points at the Antarctic-ice-shelf-wide scale.

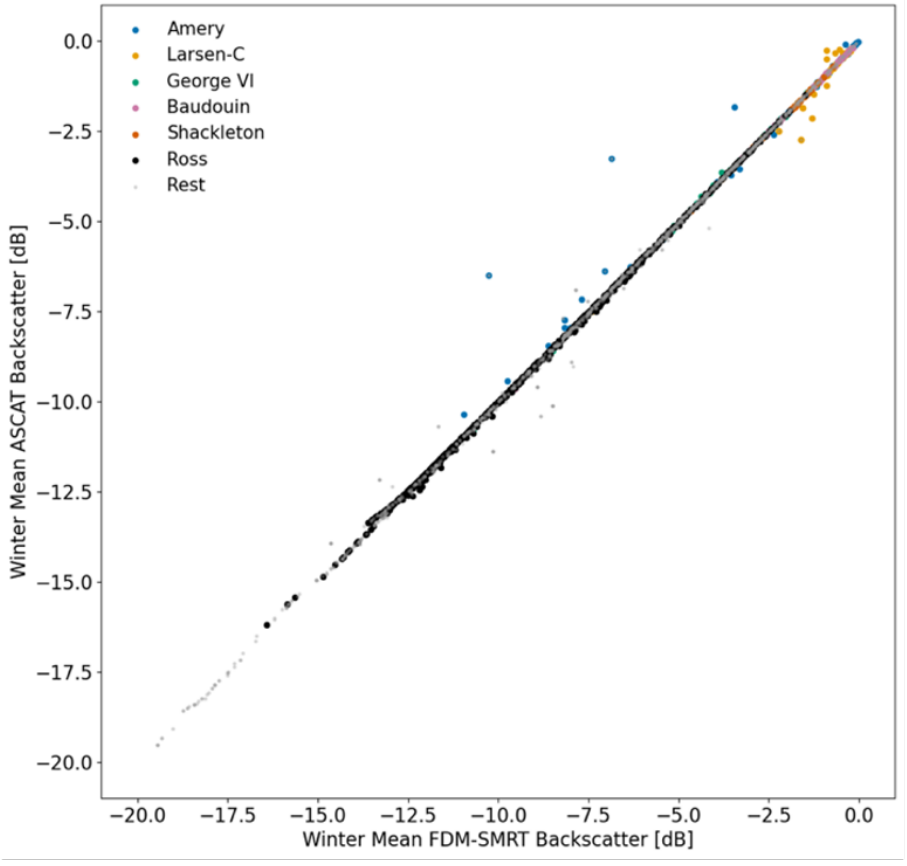

Figure A1. Absolute comparison of backscatter between winter mean FDM-SMRT coupled simulation and winter mean ASCAT observations after optimization. Pearson correlation coefficient (R-value) is 0.99 and Root Mean Squared Error (RMSE) is 0.18 dB

Appendix B: ANOVA Spatial Maps: IMAU-FDM Grain Size vs Optimized Grain Size

Fig. B1 presents a side–by–side comparison of the ANOVA partitioning of ASCAT backscatter variance using the IMAU-FDM modeled grain size (panels a–d) versus our optimized grain size (panels e–h).

In Fig. B1a, the explained variance due to r_{FDM} shows a spatially heterogeneous pattern, with certain regions in West Antarctica exhibiting moderate contributions. By contrast, Fig. B1e demonstrates that after optimization, grain size (r_{Opt}) explains a much larger fraction of ASCAT backscatter variability, especially across the dry ice shelf regions of the West

https://doi.org/10.5194/egusphere-2026-1263
Preprint. Discussion started: 7 April 2026

Antarctica and the East Antarctica, and portions of the Antarctic Peninsula. These regions fall into intermediate – high FAC regime (i.e., ≈ 12 - 25 m FAC in Fig. 1b, representing the right side of the inverted U-curve), where our optimized grain size accounts for backscatter variability more consistently within the adopted framework.

By construction, part of the variance increase is expected: r_{Opt} is obtained by fitting SMRT to ASCAT year by year, so variance that previously sat with FAC or the residual is reallocated to r_{Opt} where backscatter is grain-size sensitive. Beyond this, a plausible physical contributor in dry-snow regimes is episodic refreezing that enlarges grains (Veldhuijsen et al., 2024). This unidirectional increase in grain size can still cause noticeable interannual changes in backscatter (Picard et al., 2022b; Fraser et al., 2016), as regions with smaller initial grains experience more pronounced growth compared to regions where grains are already large and relatively less influenced by refreezing (Veldhuijsen et al., 2024).

Fig. B1b highlights the variance explained by FAC, which is concentrated over specific regions, such as parts of Ross and Filchner-Ronne ice shelves but remains generally low across the ice shelves. After optimization, the relative contribution of FAC to backscatter variance (Fig. B1f) falls well below its pre-optimization levels. This drop occurs because the optimized grain-size term now absorbs much of the variability that was captured by FAC variation when modelled grain sizes were used. However, depleted firn regions near the grounding line of Amery, Larsen-B, and George-VI ice shelves still exhibit relatively high explained variance. This indicates that regions in the left side of the inverted U-curve display enhanced sensitivity of ASCAT backscatter to FAC variations. From a physical perspective, we expect depleted regions to have larger grains where the density reaches the density of the glacial ice. This thus limits further grain growth and results in almost no scattering interfaces for the incoming radar signal. In such cases, changes in grain size have a negligible effect on backscatter, as also demonstrated in Fig. 2. Fig. B1c demonstrates the combined (shared) variance explained by FAC and r_{FDM}, showing only limited interaction between the two, especially in regions of West Antarctic ice shelves. In Fig. B1g, this combined effect, after optimization, further reduces the explained variance in localized regions where firn processes are more dynamic, such as near the grounding lines of ice shelves and in areas of higher surface activity.

The most striking result is shown in Fig. B1d, where the unexplained variance dominates across the Antarctic ice shelves. This indicates that before optimization neither grain size, FAC, nor their shared influence can account for a significant portion of the interannual variability in the ASCAT backscatter signal. However, notably, in Fig. B1h, the unexplained variance after optimization has decreased substantially compared to the earlier results in Fig. B1d. While regions with high unexplained variance persist (particularly in isolated parts of the Antarctic Peninsula, Ross and Roi Baudouin ice shelves), the overall reduction highlights the effectiveness of grain size optimization in capturing ASCAT backscatter variability.

Appendix C: Relationship between FAC and Grain Size

Before assessing the FAC directly from ASCAT backscatter, we compared the spatial variability in IMAU-FDM winter mean grain size and optimized grain size as a function of IMAU-FDM winter mean FAC, as in Fig. C1. In regions with high FAC ($>$ 20 m), the optimized grain size remains low and closely aligns with IMAU-FDM grain size. This likely reflects limited melt in these areas, which typically maintain a dry snowpack that is well represented by IMAU-FDM. At intermediate

https://doi.org/10.5194/egusphere-2026-1263
Preprint. Discussion started: 7 April 2026

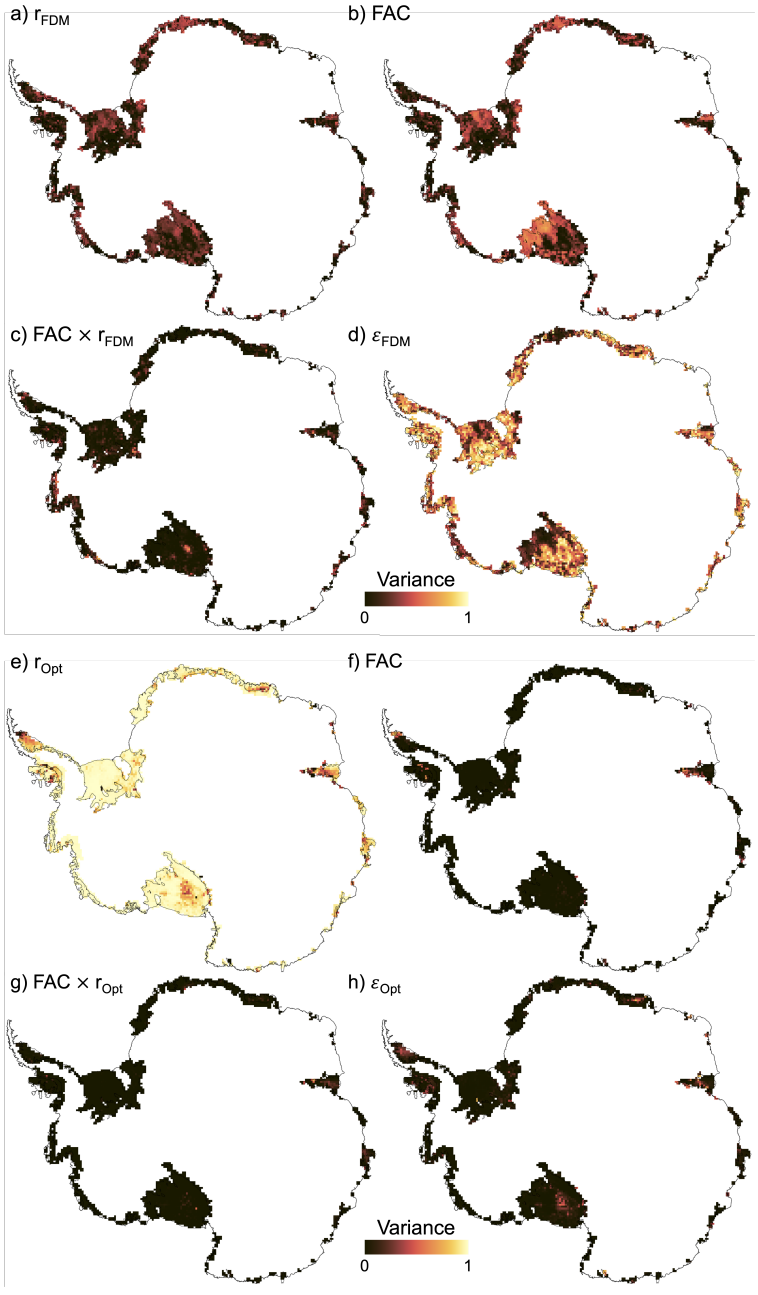

Figure B1. Spatial maps of the fraction of ASCAT backscatter variance explained by FAC, grain size (r) and their interaction, before and after grain–size optimization. Panels (a–d) show ANOVA using IMAU-FDM model grain size ($\mathrm{r_{FDM}}$): (a) contribution of $\mathrm{r_{FDM}}$, (b) of FAC, (c) their shared FAC×$\mathrm{r_{FDM}}$ term, and (d) unexplained variance ($\varepsilon_{\mathrm{FDM}}$). Panels (e–h) show the same decomposition after replacing $\mathrm{r_{FDM}}$ with our ASCAT-optimized grain size ($\mathrm{r_{Opt}}$): (e) $\mathrm{r_{Opt}}$, (f) FAC, (g) FAC×$\mathrm{r_{Opt}}$, and (h) unexplained variance ($\varepsilon_{\mathrm{Opt}}$).

https://doi.org/10.5194/egusphere-2026-1263
Preprint. Discussion started: 7 April 2026

FAC (5-20 m), IMAU-FDM generally predicts smaller grain sizes, while the optimized estimates show a wider spread. For ice shelves experiencing episodic melt within this range, enhanced refreezing and metamorphism can yield coarser effective microstructure, which IMAU-FDM's fixed 0.25 mm refreeze-grain-size parameterization (and its limited representation of repeated melt–refreeze cycles) may not fully capture (Veldhuijsen et al., 2024). In strongly depleted firn (FAC < 5 m), grain size often increases substantially in both the optimized and modeled cases, consistent with dense, refrozen firn and ice-saturated conditions.

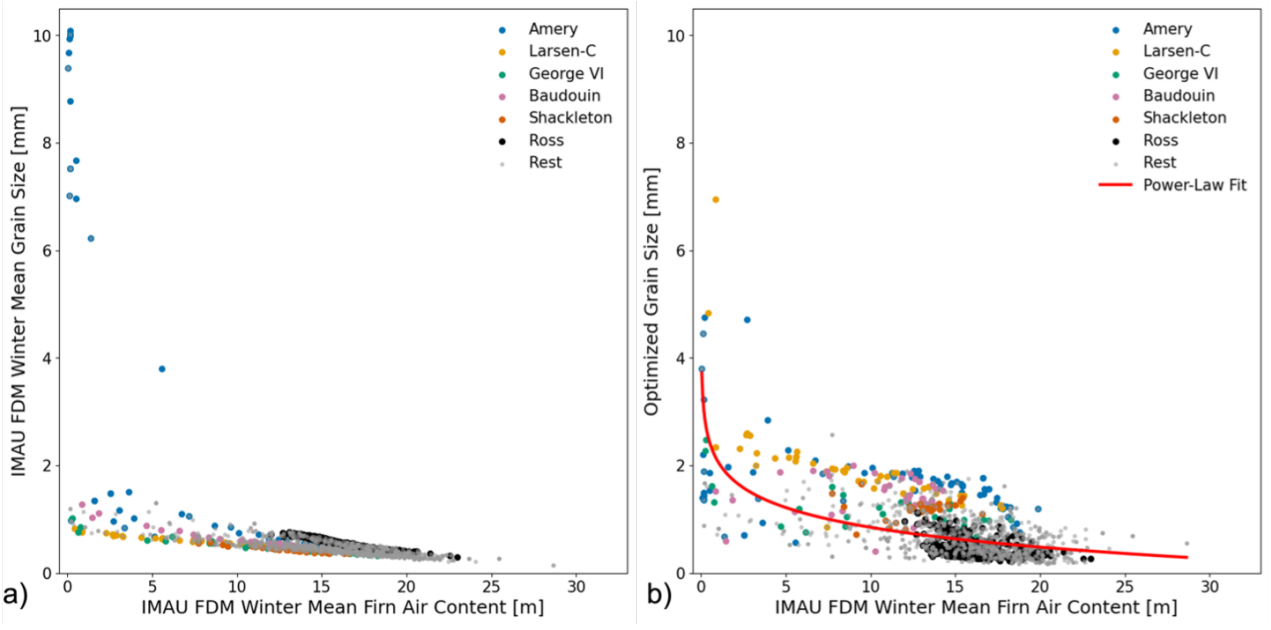

Figure C1. Antarctic-ice-shelf-wide relationship between IMAU-FDM winter mean FAC and a) IMAU-FDM winter mean grain size, b) Optimized grain size (power law fit represented by red line). 'Rest' represents the data points of all other ice shelves except the ones mentioned in color.

Author contributions. SS, BW, and SL defined the research goals and designed the study. SS performed the AIS-wide scale FDM-SMRT simulations, developed the optimization scheme, designed the visualizations used in the manuscript, and analysed the results. SV provided all IMAU-FDM profiles and data products and helped in analysing the results. SdRH helped in accessing the Antarctic-ice-shelf-wide scale ASCAT data for the period 2007 – 2021. WL helped in analysing the results and providing input to the optimization algorithm. All authors contributed to discussions on the paper.

Competing interests. The authors declare that they have no known competing financial interests or personal relationships that could have appeared to influence the work reported in this paper.

https://doi.org/10.5194/egusphere-2026-1263
Preprint. Discussion started: 7 April 2026

Disclaimer. Publisher's note: Copernicus Publications remains neutral with regard to jurisdictional claims made in the text, published maps, institutional affiliations, or any other geographical representation in this paper. The authors bear the ultimate responsibility for providing appropriate place names. Views expressed in the text are those of the authors and do not necessarily reflect the views of the publisher.

Acknowledgements. The authors acknowledge the use of computational resources of the DelftBlue supercomputer, provided by Delft High Performance Computing Centre (https://www.tudelft.nl/dhpc). We also want to thank Dr. Harish Baki for his support in DelftBlue supercomputer processing. During the preparation of this work, the authors used ChatGPT in order to enhance the readability of specific sections. After using this tool, the authors reviewed and edited the content as needed and take full responsibility for the content of the publication.

Financial support. The work of Shashwat Shukla, Sophie de Roda Husman, and Sanne Veldhuijsen was supported by Nederlandse Organisatie voor Wetenschappelijk Onderzoek (NWO) under grant no. OCENW.GROOT.2019.091. The work of Weiran Li was supported by the NWO through the ENW.GO.001.040 project.

https://doi.org/10.5194/egusphere-2026-1263
Preprint. Discussion started: 7 April 2026

References

Alley, K., Scambos, T., Miller, J., Long, D., and MacFerrin, M.: Quantifying vulnerability of Antarctic ice shelves to hydrofracture using microwave scattering properties, Remote Sensing of Environment, 210, 297–306, https://doi.org/https://doi.org/10.1016/j.rse.2018.03.025, 2018.

Amory, C., Buizert, C., Buzzard, S., Case, E., Clerx, N., Culberg, R., Datta, R. T., Dey, R., Drews, R., Dunmire, D., Eayrs, C., Hansen, N., Humbert, A., Kaitheri, A., Keegan, K., Kuipers Munneke, P., Lenaerts, J. T. M., Lhermitte, S., Mair, D., McDowell, I., Mejia, J., Meyer, C. R., Morris, E., Moser, D., Oraschewski, F. M., Pearce, E., de Roda Husman, S., Schlegel, N.-J., Schultz, T., Simonsen, S. B., Stevens, C. M., Thomas, E. R., Thompson-Munson, M., Wever, N., Wouters, B., and team, T. F. S.: Firn on ice sheets, Nature Reviews Earth & Environment, 5, 79–99, https://doi.org/10.1038/s43017-023-00507-9, 2024.

Arioli, S., Picard, G., Arnaud, L., and Favier, V.: Dynamics of the snow grain size in a windy coastal area of Antarctica from continuous in situ spectral-albedo measurements, The Cryosphere, 17, 2323–2342, https://doi.org/10.5194/tc-17-2323-2023, 2023.

Brucker, L., Picard, G., and Fily, M.: Snow grain-size profiles deduced from microwave snow emissivities in Antarctica, Journal of Glaciology, 56, 514–526, https://doi.org/10.3189/002214310792447806, 2010.

Cartwright, J., Fraser, A. D., and Porter-Smith, R.: Polar maps of C-band backscatter parameters from the Advanced Scatterometer, Earth System Science Data, 14, 479–490, https://doi.org/10.5194/essd-14-479-2022, 2022.

Charrois, L., Cosme, E., Dumont, M., Lafaysse, M., Morin, S., Libois, Q., and Picard, G.: On the assimilation of optical reflectances and snow depth observations into a detailed snowpack model, The Cryosphere, 10, 1021–1038, https://doi.org/10.5194/tc-10-1021-2016, 2016.

Clerx, N., Machguth, H., Tedstone, A., Jullien, N., Wever, N., Weingartner, R., and Roessler, O.: In situ measurements of melt-water flow through snow and firn in the accumulation zone of the SW Greenland Ice Sheet, The Cryosphere, 16, 4379–4401, https://doi.org/10.5194/tc-16-4379-2022, 2022.

Cluzet, B., Revuelto, J., Lafaysse, M., Tuzet, F., Cosme, E., Picard, G., Arnaud, L., and Dumont, M.: Towards the assimilation of satellite reflectance into semi-distributed ensemble snowpack simulations, Cold Regions Science and Technology, 170, 102 918, https://doi.org/https://doi.org/10.1016/j.coldregions.2019.102918, 2020.

Dattler, M. E., Medley, B., and Stevens, C. M.: A physics-based Antarctic melt detection technique: combining Advanced Microwave Scanning Radiometer 2, radiative-transfer modeling, and firn modeling, The Cryosphere, 18, 3613–3631, https://doi.org/10.5194/tc-18-3613-2024, 2024.

Delft High Performance Computing Centre (DHPC): DelftBlue Supercomputer (Phase 2), https://www.tudelft.nl/dhpc/ark:/44463/DelftBluePhase2, 2024.

Fraser, A. D., Nigro, M. A., Ligtenberg, S. R. M., Legresy, B., Inoue, M., Cassano, J. J., Kuipers-Munneke, P., Lenaerts, J. T. M., Young, N. W., Treverrow, A., and et al.: Drivers of ASCAT C band backscatter variability in the dry snow zone of Antarctica, Journal of Glaciology, 62, 170–184, https://doi.org/10.1017/jog.2016.29, 2016.

Gelman, A.: Analysis of variance—why it is more important than ever, The Annals of Statistics, 33, 1–53, 2005.

Greene, C. A., Gardner, A. S., Schlegel, N.-J., and Fraser, A. D.: Antarctic calving loss rivals ice-shelf thinning, Nature, 609, 948–953, https://doi.org/10.1038/s41586-022-05037-w, 2022.

Kuipers Munneke, P., Ligtenberg, S. R., Van Den Broeke, M. R., and Vaughan, D. G.: Firn air depletion as a precursor of Antarctic ice-shelf collapse, Journal of Glaciology, 60, 205–214, https://doi.org/10.3189/2014JoG13J183, 2014.

https://doi.org/10.5194/egusphere-2026-1263
Preprint. Discussion started: 7 April 2026

Ligtenberg, S. R. M., Kuipers Munneke, P., and van den Broeke, M. R.: Present and future variations in Antarctic firn air content, The Cryosphere, 8, 1711–1723, https://doi.org/10.5194/tc-8-1711-2014, 2014.

Long, D., Hardin, P., and Whiting, P.: Resolution enhancement of spaceborne scatterometer data, IEEE Transactions on Geoscience and Remote Sensing, 31, 700–715, https://doi.org/10.1109/36.225536, 1993.

Medley, B., Neumann, T. A., Zwally, H. J., Smith, B. E., and Stevens, C. M.: Simulations of firn processes over the Greenland and Antarctic ice sheets: 1980–2021, The Cryosphere, 16, 3971–4011, https://doi.org/10.5194/tc-16-3971-2022, 2022.

Moussavi, M., Pope, A., Halberstadt, A. R. W., Trusel, L. D., Cioffi, L., and Abdalati, W.: Antarctic Supraglacial Lake Detection Using Landsat 8 and Sentinel-2 Imagery: Towards Continental Generation of Lake Volumes, Remote Sensing, 12, https://doi.org/10.3390/rs12010134, 2020.

Mätzler, C.: Relation between grain-size and correlation length of snow, Journal of Glaciology, 48, 461–466, https://doi.org/10.3189/172756502781831287, 2002.

Noël, B., van Wessem, J. M., Wouters, B., Trusel, L., Lhermitte, S., and van den Broeke, M. R.: Higher Antarctic ice sheet accumulation and surface melt rates revealed at 2 km resolution, Nature Communications, 14, 7949, https://doi.org/10.1038/s41467-023-43584-6, 2023.

Pan, J., Durand, M. T., Vander Jagt, B. J., and Liu, D.: Application of a Markov Chain Monte Carlo algorithm for snow water equivalent retrieval from passive microwave measurements, Remote Sensing of Environment, 192, 150–165, https://doi.org/https://doi.org/10.1016/j.rse.2017.02.006, 2017.

Pfeffer, W. T., Meier, M. F., and Illangasekare, T. H.: Retention of Greenland runoff by refreezing: Implications for projected future sea level change, Journal of Geophysical Research: Oceans, 96, 22 117–22 124, https://doi.org/https://doi.org/10.1029/91JC02502, 1991.

Picard, G., Sandells, M., and Löwe, H.: SMRT: an active–passive microwave radiative transfer model for snow with multiple microstructure and scattering formulations (v1.0), Geoscientific Model Development, 11, 2763–2788, https://doi.org/10.5194/gmd-11-2763-2018, 2018.

Picard, G., Löwe, H., and Mätzler, C.: Brief communication: A continuous formulation of microwave scattering from fresh snow to bubbly ice from first principles, The Cryosphere, 16, 3861–3866, https://doi.org/10.5194/tc-16-3861-2022, 2022a.

Picard, G., Löwe, H., Domine, F., Arnaud, L., Larue, F., Favier, V., Le Meur, E., Lefebvre, E., Savarino, J., and Royer, A.: The Microwave Snow Grain Size: A New Concept to Predict Satellite Observations Over Snow-Covered Regions, AGU Advances, 3, e2021AV000 630, https://doi.org/https://doi.org/10.1029/2021AV000630, e2021AV000630 2021AV000630, 2022b.

Poizat, M., Picard, G., Arnaud, L., Narteau, C., Amory, C., and Brun, F.: Widespread longitudinal snow dunes in Antarctica shaped by sintering, Nature Geoscience, 17, 889–895, https://doi.org/10.1038/s41561-024-01506-1, 2024.

Scambos, T., Hulbe, C., and Fahnestock, M.: Climate-Induced Ice Shelf Disintegration in the Antarctic Peninsula, pp. 79–92, American Geophysical Union (AGU), ISBN 9781118668450, https://doi.org/https://doi.org/10.1029/AR079p0079, 2003.

Scambos, T. A., Hulbe, C., Fahnestock, M., and Bohlander, J.: The link between climate warming and break-up of ice shelves in the Antarctic Peninsula, Journal of Glaciology, 46, 516–530, https://doi.org/10.3189/172756500781833043, 2000.

Shukla, S., Wouters, B., Picard, G., Wever, N., Izeboud, M., Husman, S. d. R., Kausch, T., Veldhuijsen, S., Mätzler, C., and Lhermitte, S.: Large Variability in Dominant Scattering From Sentinel-1 SAR in East Antarctica: Challenges and Opportunities, IEEE Journal of Selected Topics in Applied Earth Observations and Remote Sensing, 17, 14 380–14 393, https://doi.org/10.1109/JSTARS.2024.3438233, 2024.

Tedesco, M. and Kim, E.: Retrieval of dry-snow parameters from microwave radiometric data using a dense-medium model and genetic algorithms, IEEE Transactions on Geoscience and Remote Sensing, 44, 2143–2151, https://doi.org/10.1109/TGRS.2006.872087, 2006.

https://doi.org/10.5194/egusphere-2026-1263
Preprint. Discussion started: 7 April 2026

van Dalum, C. T., van de Berg, W. J., and van den Broeke, M. R.: Sensitivity of Antarctic surface climate to a new spectral snow albedo and radiative transfer scheme in RACMO2.3p3, The Cryosphere, 16, 1071–1089, https://doi.org/10.5194/tc-16-1071-2022, 2022.

van Wessem, J., van den Broeke, M. R., Lhermitte, S., and Wouters, B.: Data set: Yearly RACMO2.3p2 variables, threshold temperature and Sentinel-2 melt pond volume, https://doi.org/10.5281/zenodo.7334047, 2022.

van Wessem, J. M., van de Berg, W. J., Noël, B. P. Y., van Meijgaard, E., Amory, C., Birnbaum, G., Jakobs, C. L., Krüger, K., Lenaerts, J. T. M., Lhermitte, S., Ligtenberg, S. R. M., Medley, B., Reijmer, C. H., van Tricht, K., Trusel, L. D., van Ulft, L. H., Wouters, B., Wuite, J., and van den Broeke, M. R.: Modelling the climate and surface mass balance of polar ice sheets using RACMO2 – Part 2: Antarctica (1979–2016), The Cryosphere, 12, 1479–1498, https://doi.org/10.5194/tc-12-1479-2018, 2018.

van Wessem, J. M., van den Broeke, M. R., Wouters, B., and Lhermitte, S.: Variable temperature thresholds of melt pond formation on Antarctic ice shelves, Nature Climate Change, 13, 161–166, https://doi.org/10.1038/s41558-022-01577-1, 2023.

Veldhuijsen, S.: IMAU-FDM v12AD TC release, https://doi.org/10.5281/zenodo.10723570, 2024.

Veldhuijsen, S. B. M., van de Berg, W. J., Brils, M., Kuipers Munneke, P., and van den Broeke, M. R.: Characteristics of the 1979–2020 Antarctic firn layer simulated with IMAU-FDM v1.2A, The Cryosphere, 17, 1675–1696, https://doi.org/10.5194/tc-17-1675-2023, 2023.

Veldhuijsen, S. B. M., van de Berg, W. J., Kuipers Munneke, P., and van den Broeke, M. R.: Firn air content changes on Antarctic ice shelves under three future warming scenarios, The Cryosphere, 18, 1983–1999, https://doi.org/10.5194/tc-18-1983-2024, 2024.

Virtanen, P., Gommers, R., Oliphant, T. E., Haberland, M., Reddy, T., Cournapeau, D., Burovski, E., Peterson, P., Weckesser, W., Bright, J., van der Walt, S. J., Brett, M., Wilson, J., Millman, K. J., Mayorov, N., Nelson, A. R. J., Jones, E., Kern, R., Larson, E., Carey, C. J., Polat, İ., Feng, Y., Moore, E. W., VanderPlas, J., Laxalde, D., Perktold, J., Cimrman, R., Henriksen, I., Quintero, E. A., Harris, C. R., Archibald, A. M., Ribeiro, A. H., Pedregosa, F., van Mulbregt, P., Vijaykumar, A., Bardelli, A. P., Rothberg, A., Hilboll, A., Kloeckner, A., Scopatz, A., Lee, A., Rokem, A., Woods, C. N., Fulton, C., Masson, C., Häggström, C., Fitzgerald, C., Nicholson, D. A., Hagen, D. R., Pasechnik, D. V., Olivetti, E., Martin, E., Wieser, E., Silva, F., Lenders, F., Wilhelm, F., Young, G., Price, G. A., Ingold, G.-L., Allen, G. E., Lee, G. R., Audren, H., Probst, I., Dietrich, J. P., Silterra, J., Webber, J. T., Slavič, J., Nothman, J., Buchner, J., Kulick, J., Schönberger, J. L., de Miranda Cardoso, J. V., Reimer, J., Harrington, J., Rodríguez, J. L. C., Nunez-Iglesias, J., Kuczynski, J., Tritz, K., Thoma, M., Newville, M., Kümmerer, M., Bolingbroke, M., Tartre, M., Pak, M., Smith, N. J., Nowaczyk, N., Shebanov, N., Pavlyk, O., Brodtkorb, P. A., Lee, P., McGibbon, R. T., Feldbauer, R., Lewis, S., Tygier, S., Sievert, S., Vigna, S., Peterson, S., More, S., Pudlik, T., Oshima, T., Pingel, T. J., Robitaille, T. P., Spura, T., Jones, T. R., Cera, T., Leslie, T., Zito, T., Krauss, T., Upadhyay, U., Halchenko, Y. O., Vázquez-Baeza, Y., and 1.0 Contributors, S.: SciPy 1.0: fundamental algorithms for scientific computing in Python, Nature Methods, 17, 261–272, https://doi.org/10.1038/s41592-019-0686-2, 2020.

Xu, H., Medley, B., Tsang, L., Johnson, J. T., Jezek, K. C., Brogioni, M., and Kaleschke, L.: Polar firn properties in Greenland and Antarctica and related effects on microwave brightness temperatures, The Cryosphere, 17, 2793–2809, https://doi.org/10.5194/tc-17-2793-2023, 2023.